16

Diffusing-wave spectroscopy

David A. Weitz and David J. Pine

'There's light enough for what I've got to do'
Charles Dickens (Bill Sikes) 1812–1870

16.1 Introduction

In this chapter we describe a recent development in dynamic light scattering (DLS), which may ultimately have a significant impact on the range of problems that can be addressed and on the types of system that can be studied. We discuss diffusing-wave spectroscopy (DWS), which extends DLS to very highly multiple scattering media. This technique extends the analytic power of DLS to opaque samples such as concentrated suspensions, obviating the need to dilute or index-match. In addition, DWS opens new and exciting possibilities for studying particle dynamics on length scales that are unattainable using conventional methods. We present a summary of the theoretical principles underlying DWS, and discuss its applications, both in extending traditional DLS techniques and in studying new physical phenomena. The development of DWS is still in its relatively early stages, and considerably more work is needed to exploit this technique fully. Our goal here is to provide a comprehensive introduction to the underlying principles, and to provide some examples illustrating the great promise of DWS, in the hope of making further work more productive.

Diffusing-wave spectroscopy is very similar to conventional dynamic light scattering. Both entail the detection of the intensity of a single speckle spot of the scattered light and a measurement of its temporal fluctuations. In both cases these fluctuations are characterized by their temporal autocorrelation function, and in both cases these intensity fluctuations reflect the dynamics of the scattering medium.

In traditional DLS, the characteristic decay time of the correlation function is related to the dynamics of the medium through the length scale set by the inverse of the scattering wave vector, q^{-1}. Motion of the scatterers on this length scale leads to a change in the path length of the scattered light by one wavelength, resulting in a change in the phase of the detected light by 2π, and hence to a change in the intensity of the scattered light. Analysis of the experimentally measured autocorrelation function provides a characteristic time-scale for the intensity fluctuations. To obtain meaningful information about the dynamics of the medium from this characteristic time-scale requires knowledge of the length scale set by the scattering wave vector. It is this requirement that has limited the application of traditional DLS to the strictly single scattering limit. If light is scattered even a second time, the intermediate scattering wavevector is unknown, precluding simple, meaningful interpretation of the measured decay time of the autocorrelation function of the scattered light. Diffusing-wave spectroscopy approaches the problem of multiple scattering from an entirely different limit, that of very high multiple scattering. In this limit, the light does not undergo only one or even a small number of scattering events, but instead is scattered a *very* large number of times. In this limit, the direction of the light is totally randomized. Then the propagation of the light and the effects of the dynamics of the scattering medium can both be treated with *statistical* approximations. This approach obviates the complexity inherent in exact treatments of DLS with double or triple scattering events, and allows useful information to be obtained relatively simply from the intensity fluctuations of the scattered light in the high multiple-scattering limit.

The decay of the temporal autocorrelation function of the multiply-scattering light measured with DWS results from a change in phase of the scattered light by $\approx \pi$, just as for conventional DLS. In DWS the total path length of the light through the sample must change by one wavelength to cause the change in phase and thus the fluctuation in the intensity. The calculation of this phase change, and hence the temporal autocorrelation function in DWS, entails two fundamental approximations. The first approximation is in the description of the light propagation through the scattering medium. In the limit of very high multiple scattering, each photon is scattered a very large number of times, and its path can be described as a random walk. The simplest description of the light propagation is with the diffusion approximation.[1] This approximation neglects any interference effects of the light as it propagates through the scattering medium, and assumes that the light intensity diffuses. The neglect of interference effects within the medium is predicated on the assumption that the light scattering is not so strong as to approach the localization of light due to random scattering. It is an excellent approximation in virtually every instance of practical importance. The use of the diffusion approximation makes it possible to calculate the distribution of paths taken by the photons propagating through the medium.

The second fundamental approximation inherent in DWS is in the treatment of the effect of the dynamics of the scatterers on the phase of the light. Since each photon is scattered a large number of times as it is transported through the medium, the details of individual scattering events play a less critical role. In particular, the conservation of scattering momentum at every point along the full path can be neglected. Instead, the individual scattering events are approximated by the contribution of an average scattering event. Then the knowledge of the path length obtained through the use of the diffusion approximation determines the number of these average scattering events that

contribute to each path. It is these two approximations that make the DWS approach tractable, and allow calculation of the autocorrelation function.

The diffusion approximation has been quite widely used to describe the propagation of light through very highly scattering media. It was used as early as 1905 to describe the propagation of light through clouds. Radiation transfer theory is a well-developed description of the propagation of light through highly scattering media that reduces to the diffusion approximation under appropriate conditions. More recently, the diffusion approximation has formed the basis for the description of the transport of light through highly scattering media as the localizaton of classical waves is approached. Most treatments of the enhancement of backscattered light, or weak localization, rely on the diffusion approximation. In fact it is the experimental observation that the strong localization of light is so difficult to achieve that gives the diffusion approximation its wide applicability. Strong location of light has not been observed to date, reflecting the fact that most materials simply do not scatter strongly enough. As a consequence, the diffusion approximation provides an excellent, and very widely applicable, description of light propagation. Diffusing-wave spectroscopy is an extension of the diffusion approximation to dynamic light scattering.

Within the diffusion approximation, light propagation is parametrized by the diffusion coefficient for light, $D_l = vl^*/3$, where v is the speed of light in the medium and l^* is the transport mean free path in the medium. The effective speed of light in the medium can be substantially smaller than that in a homogeneous medium.[2] A highly scattering medium often comprises nearly resonant scatterers, described by the proximity of Mie resonances. The excitation of each resonance acts effectively as an inductance, which delays the propagation of the light. The large number of these resonant scatterers encountered by the light as it propagates through the medium causes a significant reduction in the effective speed of the light. The transport mean free path, l^*, characterizes the scattering medium itself. It is the length that a photon must travel before its direction is completely randomized. This length is typically substantially larger than the scattering mean free path, l, the length that a photon must travel before it is scattered a single time. Since strong scatterers typically scatter preferentially in the forward direction, many scattering events are required before the direction is randomized, making $l^* > l$.

The use of the diffusion approximation to describe the propagation of the light determines which media can and cannot be studied using DWS. Samples that scatter light very highly, and thus have a white or milk-like appearance, are suitable. For example, concentrated samples of latex spheres can be studied with no dilution. However, the requirement that light should diffuse through the sample also leads to some restrictions in the choice of samples. Absorption becomes much more important in highly scattering samples, since the path length followed by the light is greatly increased. While the effects of absorption can easily be included in the theoretical treatment of DWS. Thus the applicablity of DWS to samples that are coloured is much more limited than to

samples than are white. Furthermore, the requirement that the light should diffuse through the sample also restricts the application of DWS to those samples that scatter highly enough. The sample must be sufficiently opaque that a negligible amount of unscattered light is transmitted through the sample. Even with these limitations, DWS greatly broadens the range of samples that can be studied using dynamic light scattering techniques. In particular, DWS can be used to study samples that it had not previously been possible to study with DLS, including a wide range of concentrated suspensions of technological importance.

The use of the diffusion approximation to describe the propagation of light ensures that the scattering wavevector, which relates the incident and detected light, has little relevance to the resultant correlation function, because the light has undergone such a large number of intermediate scattering events. Thus, unlike DLS, the angle between the incident and detected light is not important in DWS. As a consequence there are two basic experimental geometries that have proved useful. The first is backscattering, where the light is incident on one side of the sample and the scattered light is detected from the same side. The other geometry is transmission, where the light is incident on one side of the sample and the scattered light transmitted through the sample is detected. In either case, the exact angle of the detected light is not critical. However, the exact experimental geometry is critical, as it determines the length of the paths that the scattered photons follow. Thus, for example, the thickness of the sample or the diameter of the incident beam strongly affects the decay time of the autocorrelation functions.

One of the most important driving forces behind the development of traditional DLS has been its technological application in particle sizing measurements. Traditional DLS is a well-developed method for particle sizing, provided that the suspension is sufficiently dilute, or the particles are sufficiently small, for the light to be scattered only once. However, since q is known, DLS can also provide information about the distribution of particle sizes, particularly when data can be obtained at several different scattering angles. The technological application to particle sizing may also be one of the most important driving forces in the further development of DWS. Since most suspensions of technological importance are sufficiently concentrated for them to scatter very highly, DWS may provide a means of using light scattering for particle sizing in these materials without requiring dilution. However, DWS is less well developed for particle sizing. The backscattering geometry is the most convenient one for particle sizing, and it is certainly possible to obtain a measure of the average particle size that is accurate to within about 10 to 20 per cent. With further refinements, it should ultimately be possible to obtain considerably better accuracy. The transmission geometry can also be used for particle sizing but requires additional knowledge of the scattering medium, in that the transport mean free path, l^*, must be determined independently. Unlike DLS, however, the correlation functions measured with DWS cannot be inverted to determine

information directly about particle size distributions, although their effect on the correlation functions can be calculated, allowing different models to be tested. In addition, since DWS measures the dynamics of concentrated suspensions directly, interpretation of the data in terms of an average particle size is considerably more difficult, since it must also account for the effects of particle interactions, which become much more important with increasing concentration. Thus the initial application of DWS to particle sizing will be likely to have a different emphasis from traditional DLS. It will probably be more useful in monitoring such effects as the *changes* in some average size of particles as a process proceeds than in measuring the size distribution of a totally unknown sample. However, DWS is the only technique that can be used to study highly scattering, concentrated solutions without dilution, and thus will certainly find a variety of important applications.

In addition to its potential for technological applications, DWS possesses several unique features, making it possible to study phenomena and samples that simply cannot be studied any other way. One example is the study of particle motion on very short length scales. The intensity fluctuations measured with DWS arise when the pathlength of the scattered light changes by one wavelength, just as they do in the traditional DLS. In the case of DWS, however, a change in the total path length by one wavelength is caused by the cumulative motion of a very large number of scatterers. Thus each scatterer need move only a small fraction of a wavelength. Therefore, using DWS it is possible to measure the motion of micrometre-sized particles on length scales as small as a few ångströms. Particle motion on these length scales can exhibit very different physics from motion on the much larger length scales typically measured with DLS. Another unique application of DWS exploits the diffusive nature of the propagation of the light through the medium. Diffusion light samples a much larger volume of the sample than does singly scattered light. Thus it is possible to study dynamic events that are spatially or temporally rare. As an example, DWS has been used to study the dynamics associated with the ageing of foams. These dynamics involve rearrangement of the foam bubbles, which occurs randomly and intermittently in localized regions of the foam. However, since DWS can average over a large volume of the sample, it can conveniently be used to monitor the rate of this motion. Thus new physics of the foam can be studied with DWS. These are but two examples of the applications of DWS to the study of new physical phenomena.

Finally, we note that in our discussion of DWS, we must distinguish between two different types of diffusion: the diffusion of the photons and the diffusion of the scatterers. The diffusion coefficients of each are vastly different. For light, the diffusion coefficient is given by $D_l = cl^*/3$, and for a typical transport mean free path of $l^* \approx 100$ μm, we have $D_l \approx 10^8$ cm^2 s^{-1}. For the scatterers, a typical diffusion coefficient is $D_0 \approx 10^{-8}$ cm^2 s^{-1}. Thus the photons diffuse much more rapidly than the particles. As a consequence, the light traverses the sample before the particles have moved any significant distance at all, and therefore

before the paths have changed their length. Thus DWS still is an intensity fluctuation spectroscopy, a measure of the correlations of the scattered intensity at different times as the scattering particles move.

In the remainder of this chapter, we present a description of the principles underlying DWS and a description of its potential applications. The theoretical principles of DWS are discussed in Section 16.2. We begin by considering the case where the concentration of particles is large enough to produce high multiple scattering, but small enough that neither potential nor hydrodynamic interactions need be considered. This simplifies the discussion of the effects of the particle dynamics and allows us to consider the consequences of the diffusive propagation of the light. We then discuss the limitations of the diffusion approximation and consider some possible directions for improvement. This is followed by a more detailed discussion of the consequences of particle interactions, both potential and hydrodynamic, for the theoretical treatment. Section 16.3 reviews the details of some of the applications of DWS. We begin with a discussion of the experimental requirements that are particular to DWS. We then present a description of the use of DWS for particle sizing in concentrated suspensions. Next we discuss the new unique applications of DWS to the study of phenomena and systems that cannot otherwise be studied with dynamic light scattering techniques. This includes the measurement of particle motion on very short length scales and the extension of DWS to study the dynamics of foams.

16.2 Principles of DWS

16.2.1 *Overview of theory*

In order to interpret any results obtained with a DWS experiment quantitatively, we must calculate the temporal autocorrelation function of the intensity fluctuations of the scattered light. The basic prescription that we follow is, in principle, quite straightforward: We approximate the light propagation through the very highly scattering medium as a diffusive process, which allows us to determine all the different paths that a photon can take as it traverses the medium, as well as the probability that a photon will follow any given path. We then exploit the fact that a long path involves many scattering events, and approximate each individual scattering event by an average scattering event. We next replace the sum over the individual scattering events by a sum over the same number of average scattering events. This allows us to calculate the contribution of the individual paths to the correlation function. Finally, the total correlation function is determined by summing the contributions of the individual paths, weighted by the probability that a diffusing photon follows that path. This procedure makes it possible to calculate the temporal autocorrelation function in a straightforward and physically transparent manner.[3–5]
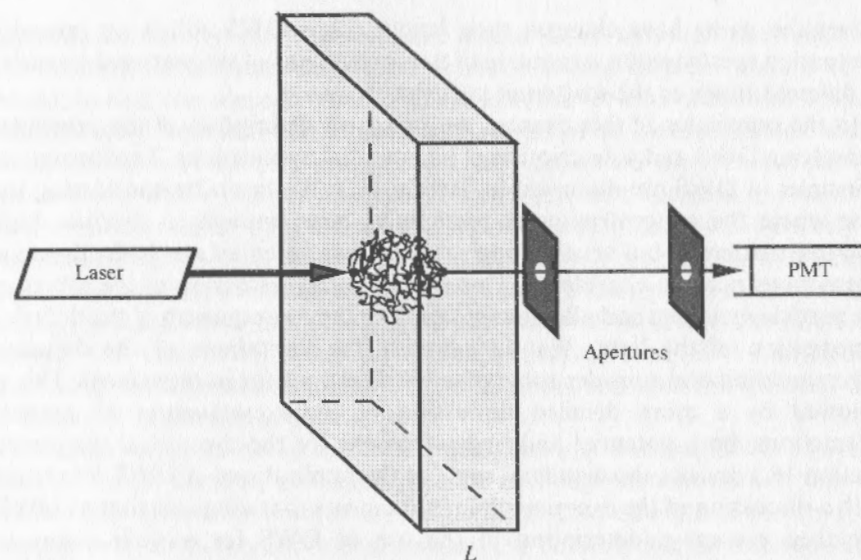
FIG. 16.1. Typical optical arrangement for DWS in the transmission geometry, showing the large number of possible diffusion paths that the photons can follow. Light is incident at a point r_{in} on the left face of the sample and is collected from a point r_{out} on the right face. The apertures defining the point r_{out} ensure that approximately one speckle of scattered light is collected. Only those paths collected by the light detector (PMT) are shown; nevertheless, there are a large number of light paths through the sample.

The approach we describe is not unique; there are other approaches that have also been used to determine the autocorrelation function, and that predate the method described here. These are based on a diagrammatic description of the light transport.[6, 7] These approaches have the advantage that they can in principle describe the behaviour when the scattering is so strong that localization of the light is approached. However, for the weaker scattering that is encountered experimentally, they reduce to the diffusion approximation used here.

To illustrate in more detail the approach that we use, it is useful to consider a specific example. We show a typical arrangement for a DWS experiment in Fig. 16.1. This is the transmission geometry, with the laser incident as a focused beam on one side of the sample, and the detected signal collected from the other side. The geometry of the sample is a slab, with a thickness L and a lateral extent much greater than the thickness. The signal detection is similar to that in a standard DLS experiment in that a single speckle spot is imaged on to a pinhole, and its fluctuating signal is analysed with a digital correlator. Again for the sake of simplicity, we begin by considering a concentrated colloidal suspension as the sample. Its concentration and scattering power must be large enough to ensure that it is milky-white in appearance, with virtually no

unscattered light transmitted through the sample. However, we initially consider a suspension whose concentration is sufficiently low that the effects of interactions, both potential and hydrodynamic, are negligible. Thus, for example, an aqueous suspension of polystyrene spheres with a volume fraction $\phi \approx 0.01$ and diameter $d \approx 0.5$ μm would be suitable.

As shown schematically in Fig. 16.1, any photon incident on one side of the sample can follow a large number of possible paths, each involving many scattering events, before it leaves the other side of the sample. The collection optics detect only a small portion of the outgoing light. Because each individual path consists of a large number of scattering events, it can be described as random walk. In the continuum limit, the diffusion equation for light can be used to describe the propagation of the light. In particular, it can be used to determined the distribution of paths of different lengths. It is this ability to calculate the distribution of path lengths using the diffusing approximation for the transport of light that is the key to DWS.

The contribution of each path to the total correlation function can also be calculated. It depends on the total number of scattering events that constitute the path, which is in turn determined by the path length and the scattering mean free path of the photons, or the average distance that a photon travels until it is scattered. The calculation of the contribution of each path is simplified by assuming that each scattering event is independent and that there are a sufficient number of scattering events in the path for the conservation of momentum for each scattering to be unimportant. Then each scattering can be represented by an average scattering event, and the contribution of the total path can be simply determined. Physically, the decay rate of the contribution of each path will be determined by how long it takes for the total path length to change by one wavelength. This in turn depends on the number of scattering events that constitute the path. The contribution of paths of different lengths will decay with different rates. However, in all cases, any individual particle will move over a length much smaller than one wavelength.

The total correlation function can be calculated by summing over the contributions of all paths, weighted by the appropriate distribution of paths determined by the diffusion equation for the light. The distribution of path lengths will be strongly dependent on geometry. Thus, for example, in transmission, the distribution of path length will depend on the thickness L of the sample and will change if the focused incident laser beam is expanded to illuminate the whole side of the sample face. Similarly, very different results will be obtained if the light is detected in the backscattering geometry, and is collected from the same face of the sample as is illuminated. By contrast, unlike traditional DLS, the measured correlation function will not depend strongly on the exact angle of detection, as in both transmission and backscattering geometries the diffusing light leaves essentially uniformly in all directions from any point on the surface of the sample.

In the remainder of this section, we describe the theory of DWS in more

detail. We concentrate initially on the physical concepts entailed in the diffusion approximation for the light transport and the statistical approach to the calculation of the contribution of each path to the total correlation function. Thus we restrict our attention to suspensions of uniform spheres with concentrations sufficiently low that interaction effects can be neglected. In this limit, we derive the functional forms for the correlation functions measured in DWS experiments for the different useful geometries. We also discuss the limitations to the diffusion approximation and describe possible methods for overcoming these limitations. We then generalize our treatment of the contribution of each path to include the effects of interactions, both in the form of potential interactions, which are characterized in terms of the structure factor of the suspension, and in terms of the hydrodynamic interactions. Both effects become important as the concentration of the suspension is increased, and thus play a critical role in the use of DWS. Finally we also generalize the assumption of scattering from a suspension of uniform spheres, and discuss the effects of polydispersity in the size of the scatterers.

16.2.2 *Simple case of single scattering*

Before developing the theory of diffusing-wave spectroscopy, we review a simple conventional dynamic light scattering experiment: Brownian diffusion in a monodisperse suspension of non-interacting colloidal spheres. Laser light with an incident wavevector k_0 illuminates the sample and, if the concentration of colloidal particles is dilute enough, is scattered no more than once before passing through the sample. Light that is scattered through an angle θ with a wavevector k_s is then detected in the far field. If the scattered field at the detector from a single particle is E_0, then the total field E is the superposition of scattered fields from all N particles in the scattering volume:

$$E(t) = \sum_{i=1}^{N} E_0 \exp[i\boldsymbol{q} \cdot \boldsymbol{r}_i(t)] \tag{16.1}$$

where $\boldsymbol{q}$ is the scattering wavevector defined by $\boldsymbol{q} = k_s - k_0$ and $\boldsymbol{r}_i(t)$ is the position of the ith particle. The argument of the exponential represents the phase shift introduced by scattering and depends on the position of each particle in the scattering volume. As the particles in the scattering volume move, the phase of the scattered field from each particle changes, causing the scattered *intensity* to fluctuate in time. Thus the rate at which the intensity fluctuates is directly determined by the motion of the particles. These fluctuations can be characterized by their temporal autocorrelation function,

$$g_{(2)}(t) \equiv \frac{1}{\beta}\left(\frac{\langle I(t)I(0)\rangle}{\langle I\rangle^2} - 1\right) = \left(\frac{\langle E(0)E^*(t)\rangle}{\langle|E|^2\rangle}\right)^2 \equiv |g_{(1)}(t)|^2, \tag{16.2}$$

where β is a constant determined primarily by the collection optics of the

experiment. The second equality in eqn (16.2) holds in many cases of experimental interest and is known as the Siegert relation. In general, the field autocorrelation function is given by[8]

$$g_{(1)}(t) = \frac{\sum_{i=1}^{N} \sum_{j=1}^{N} \langle \exp\{i\boldsymbol{q} \cdot [\boldsymbol{r}_i(0) - \boldsymbol{r}_j(t)]\}\rangle}{\sum_{i=1}^{N} \sum_{j=1}^{N} \langle \exp\{i\boldsymbol{q} \cdot [\boldsymbol{r}_i(0) - \boldsymbol{r}_j(0)]\}\rangle}. \tag{16.3}$$

For the case of non-interacting uncorrelated particles, the cross-terms $i \neq j$ vanish to give

$$g_{(1)}(t) = \langle \exp[-i\boldsymbol{q} \cdot \Delta\boldsymbol{r}(t)]\rangle, \tag{16.4}$$

where $\Delta\boldsymbol{r}(t) \equiv \boldsymbol{r}(t) - \boldsymbol{r}(0)$. Thus $g_{(1)}(t)$ decays appreciably when $\boldsymbol{q} \cdot \Delta\boldsymbol{r}(t) \simeq \pi$, or, equivalently, when $\Delta r \approx \lambda$. If $\Delta\boldsymbol{r}(t)$ is a Gaussian random variable, then

$$g_{(1)}(t) = \exp[-q^2\langle\Delta r^2(t)\rangle/6]. \tag{16.5}$$

For simple diffusion, $\langle\Delta r^2(t)\rangle = 6Dt$, where D is the particle diffusion coefficient, and we obtain

$$g_{(1)}(t) = \exp(-q^2 Dt). \tag{16.6}$$

In this case the autocorrelation function decays exponentially with a time constant $\tau = 1/Dq^2$.

16.2.3 *Multiple scattering and the diffusion approximation*

In the multiple scattering limit, there are two length scales which characterize light scattering and transport: the mean free path l between scattering events, and the transport mean free path l^*. The mean free path is the average distance between scattering events and, in dilute suspensions, is given by[1]

$$l = \frac{1}{\rho\sigma}, \tag{16.7}$$

where ρ is the number density of particles and σ is the total scattering cross-section for a single particle in suspension. The transport mean free path l^* is the length scale over which the direction of light propagation is randomized; it is related to the mean free path by[1]

$$l^* = \frac{l}{\langle 1 - \cos\theta\rangle}, \tag{16.8}$$

where θ is the scattering angle and $\langle\ \rangle$ indicates an ensemble average over many scattering events. The transport mean free path takes on different values relative to the mean free path, depending upon the value of k_0a, where a is the radius of the particles and $k_0 = 2\pi/\lambda$. In the limit of small particles, when $k_0a \ll 1$, the single-particle scattering is isotropic and the direction of light is randomized after a single scattering event; in this case, $l^* = l$. For larger

particles, the scattering is typically peaked in the forward direction so that several scattering events are required, on average, to randomize the direction of propagation; in this case, $l^* > l$. The mean free path and transport mean free path can be determined experimentally by measuring the transmission coefficient T of a plane wave of light through a suspension of thickness L. If $L \lesssim l$, then $T \approx \exp(-L/l)$ and most of the transmitted light is *unscattered* light. If $L \gg l^*$, then $T \approx l^*/L$ and essentially none of the transmitted light is unscattered. In this limit, light propagation is diffusive so that photons execute a random walk of step length l^*, the length scale over which the direction of propagation is randomized. In general, several scattering events are required to randomize the direction of propagation, implying that $l \leqslant l^*$. Thus transmitted light will have undergone $\approx (L/l^*)^2$ random walk steps with (l^*/l) scattering events per step. In a typical transmission experiment, therefore, light will have been scattered on average $n \approx (L/l^*)^2(l^*/l)$ times before leaving the sample, When $L \gg l^*$, the system is considered to be in the highly multiple scattering limit. It is important to note, however, that in nearly all cases of experimental interest the scattering from each particle is sufficiently weak so that $k_0 l \gg 1$. This means that the Born approximation can be used to describe the scattering from each particle even for systems in the highly multiple scattering limit. In Fig. 16.2, l and l^* are plotted as a function of particle size for a 1 vol.% suspension of polystyrene spheres in water. The plot shows that the scattering is strongest
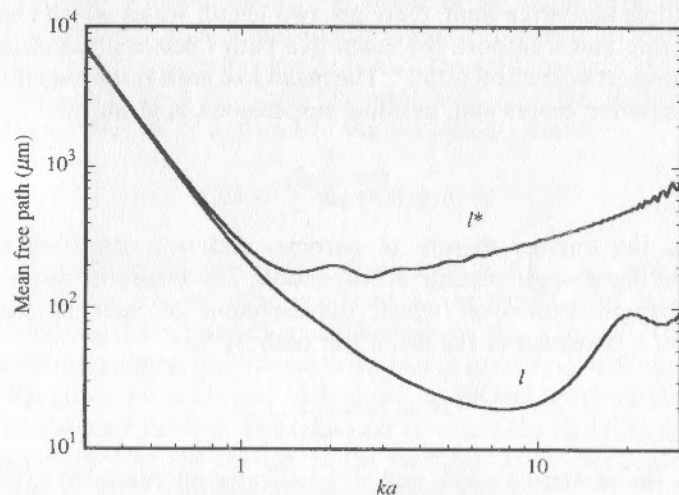

FIG. 16.2. Mean free path l and transport mean free path l^* vs. dimensionless particle size, $k_0 a$, for a 1 vol.% aqueous suspension of polystyrene spheres. The mean free paths are calculated from the formulae $l = (\rho\sigma)^{-1}$ and $l^* = l/\langle 1 - \cos\theta\rangle$, where ρ is the number density of particles, σ is the total scattering cross-section calculated from Mie scattering theory, and θ is the scattering angle. For $k_0 a \ll 1$, $l \approx l^*$; for $k_0 a \gtrsim 1$, $l < l^*$.
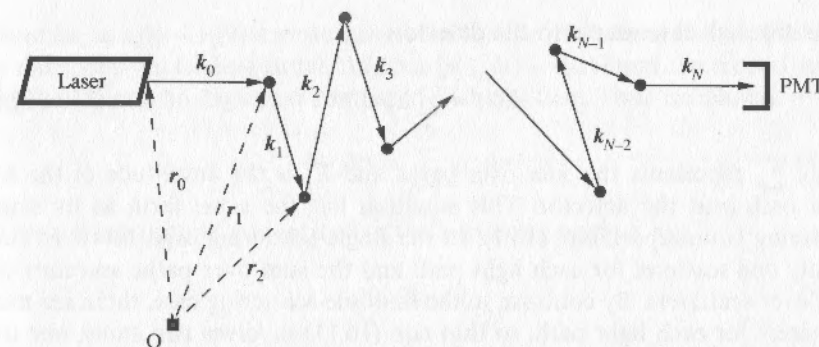
FIG. 16.3. A single path through a sample of multiply-scattered light. The wavevectors k_i have the same magnitude k_0 and the point in the direction of propagation. The position vectors r_i give the instantaneous position of the scattering particles.

when the particle size is comparable with the wavelength of light. When the particle size is much smaller than the wavelength, l and l^* become very large and the multiple scattering is relatively low.

16.2.3.1 *Autocorrelation function for multiply-scattered light.* We wish to obtain an expression for the field autocorrelation function in the highly multiple scattering limit. First we consider a DWS measurement in a transmission experiment. Light from a laser is incident on one side of a planar sample of thickness $L \gg l^*$ and scattered light is collected from a small area on the opposite side as shown in Fig. 16.1. A single photon passing through the sample undergoes n scattering events and emerges with a phase that depends on its total path length s. The geometry for a single path is illustrated in Fig. 16.3. The total path length for a photon scattering N times is

$$s = \sum_{i=0}^{N} |r_{i+1} - r_i| = \sum_{i=0}^{N} \left(\frac{k_i}{|k_i|}\right) \cdot (r_{i+1} - r_i), \quad (16.9)$$

where k_i is the wavevector of the light after i scattering events, r_i is the position of particle i for $i \leqslant 1 \leqslant n$, r_0 is the position of the source (laser), and r_{N+1} is the position of the detector (PMT), Because the scattering is quasi-elastic, all wavevectors have the same magnitude, that is, $k_i = k_0$ for all i. Thus the total phase shift $\phi(t)$ of the photon after passing from the laser to the detector is

$$\phi(t) = k_0 s(t) = \sum_{i=0}^{N} k_i(t) \cdot [r_{i+1}(t) - r_i(t)]. \quad (16.10)$$

The total field at the detector is the superposition of the fields from all light

paths through the sample to the detector:

$$E(t) = \sum_p E_p \, e^{i\phi_p(t)}, \tag{16.11}$$

where $\sum_p$ represents the sum over paths and E_p is the amplitude of the field from path p at the detector. This equation has the same form as its single-scattering counterpart, eqn (16.1). In the single-scattering case, however, there is only one scatterer for each light path and the sum over paths amounts to a sum over scatterers. By contrast, in the multiple-scattering case, there are many scatterers for each light path, so that eqn (16.11) involves two sums, one over light paths and another over the particles in each path. In addition, the field amplitude E_p is not determined simply by the laser beam intensity, as it is in the single-scattering case. Instead, E_p depends on the number of scattering events in a given path as well as the laser beam intensity. The determination of E_p adds some complexity to the multiple-scattering theory. The field autocorrelated function is obtained from eqn (16.11):

$$g_{(i)}(t) \equiv \left(\frac{\langle E(0)E^*(t)\rangle}{\langle |E|^2 \rangle} \right) = \frac{1}{\langle I \rangle} \left\langle \left(\sum_p E_p \, e^{i\phi_p(0)} \right)\left(\sum_{p'} E_{p'}^* \, e^{-i\phi_{p'}(t)} \right) \right\rangle, \tag{16.12}$$

where $\langle I \rangle$ is the *total* average scattered intensity at the detector. For independent particles, the fields from different paths are to a very good approximation uncorrelated. Thus terms with $p \neq p'$ in eqn (16.12) do not contribute, and we obtain

$$g_{(1)}(t) = \left\langle \sum_p \frac{|E_p|^2}{\langle I \rangle} \, e^{i[\phi_p(0) - \phi_p(t)]} \right\rangle$$

$$= \sum_p \frac{\langle I_p \rangle}{\langle I \rangle} \, \langle e^{i[\phi_p(0) - \phi_p(t)]} \rangle, \tag{16.13}$$

where $\langle I_p \rangle \equiv \langle |E_p|^2 \rangle$ is the average intensity from path p and we have assumed the independence of the phase and field amplitude E_p at the detector.

To make further progress, we must obtain an expression for the change in the phase of the scattered light resulting from particle motion. From eqn (16.10), we have

$$\Delta\phi_p(t) = \phi_p(t) - \phi_p(0)$$

$$= \sum_{i=0}^{N} k_i(t) \cdot [r_{i+1}(t) - r_i(t)] - \sum_{i=0}^{N} k_i(0) \cdot [r_{i+1} - r_i(0)]. \tag{16.14}$$

Defining $q_i \equiv k_i(0) - k_{i-1}(0)$ and $\Delta k_i(t) \equiv k_i(t) - k_i(0)$, we obtain

$$\Delta\phi_p(t) = \sum_{i=1}^{N} q_i \cdot \Delta r_i(t) + \sum_{i=0}^{N} \Delta k_i(t) \cdot [r_{i+1}(t) - r_i(t)], \tag{16.15}$$

where $\Delta r_i \equiv r_i(t) - r_i(0)$ and we have used the fact that the source and detector do not move. To leading order, $\Delta k_i(t) \perp [r_{i+1}(t) - r_i(t)]$ and the second sum in eqn (16.15) can be neglected compared with the first. Thus we obtain

$$\Delta\phi_p(t) = \sum_{i=1}^{N} q_i \cdot \Delta r_i(t), \tag{16.16}$$

where the magnitude q is related to the scattering angle θ by

$$q = 2k_0 \sin\frac{\theta}{2}. \tag{16.17}$$

We can evaluate the average over the phase factors in eqn (16.13) by noting that for large N, $\Delta\phi_p(t)$ is a random Gaussian variable. This follows from the central limit theorem. Thus we have

$$\langle e^{-i\Delta\phi_p(t)} \rangle = e^{-\langle \Delta\phi_p^2(t)\rangle/2}. \tag{16.18}$$

Using the expression for $\Delta\phi_p(t)$ in eqn (16.16), we obtain

$$\langle \Delta\phi_p^2(t) \rangle = \sum_{i=1}^{N} \sum_{j=1}^{N} \langle [q_i \cdot \Delta r_i(t)][q_j \cdot \Delta r_j(t)] \rangle$$

$$= \sum_{i=1}^{N} \langle [q_i \cdot \Delta r_i(t)]^2 \rangle, \tag{16.19}$$

where we have assumed the independence of successive phase factors $q_i \cdot \Delta r_i(t)$. We further assume that the scattering vector q_i and displacement vector $\Delta r_i(t)$ are independent, so that

$$\langle \Delta\phi_p^2(t) \rangle = N \langle [q_i \cdot \Delta r_i(t)]^2 \rangle$$

$$= \tfrac{1}{3} N \langle q^2 \rangle \langle \Delta r^2(t) \rangle. \tag{16.20}$$

The average over q^2 is weighted by the single-particle form factor (or differential cross-section) and can be expressed in terms of the mean free paths:

$$\langle q^2 \rangle = \langle [2k_0 \sin(\theta/2)]^2 \rangle = 2k_0^2 \langle 1 - \cos\theta \rangle = 2k_0^2 \frac{l}{l*}. \tag{16.21}$$

For long light paths where $N \gg 1$, the total path length through the sample is given by $s = Nl$. Therefore, setting $N = s/l$ and using eqn (16.21) for $\langle q^2 \rangle$, we find

$$\langle \Delta\phi_p^2(t) \rangle = \frac{1}{3}\frac{s}{l} 2k_0^2 \frac{l}{l*} \langle \Delta r^2(t) \rangle$$

$$= \frac{2}{3} k_0^2 \langle \Delta r^2(t) \rangle \frac{s}{l*}. \tag{16.22}$$

The scattering mean free path l drops out of the final expression for $\langle \Delta\phi_p^2(t) \rangle$

and the only remaining length scale that characterizes the scattering is the transport mean free path, l^*. This implies that for length scales much greater than l^*, the fluctuation spectrum of scattered light can accurately be described within the photon diffusion approximation. For diffusing colloiding particles, $\langle \Delta r^2(t) \rangle = 6Dt$ and we have

$$\langle \Delta\phi_p^2(t) \rangle = 4k_0^2 Dt \frac{s}{l^*}. \tag{16.23}$$

For large N, eqns (16.22) and (16.23) show that $\langle \Delta\phi_p^2(t) \rangle$ depends on the path length s of the light and not on any other path-dependent property. Using this result, we can recast eqn (16.13) as a sum over *path lengths* rather than a sum over individual *paths*, provided that we replace the fraction of scattered intensity in path p, $\langle I_p \rangle/\langle I \rangle$, with the fraction of scattered intensity in paths of length s, $P(s)$. Thus, from eqns (16.13), (16.18), and (16.22) we obtain

$$g_{(1)}(t) = \sum_s P(s) \exp\left(-\tfrac{1}{3}k_0^2 \langle \Delta r^2(t) \rangle \frac{s}{l^*} \right), \tag{16.24}$$

or, using eqn (16.23) for diffusive motion,

$$g_{(1)}(t) = \sum_s P(s) \exp\left(-2k_0^2 Dt \frac{s}{l^*} \right). \tag{16.25}$$

Thus the calculation of the autocorrelation function is reduced to determining the path-length distribution function $P(s)$ through a sample. This calculation is greatly facilitated by passing to the continuum limit; in this limit, eqn (16.25) becomes[3]

$$g_{(1)}(t) = \int_0^\infty P(s)\, e^{-(2t/\tau)s/l^*}\, ds, \tag{16.26}$$

where $\tau = (k_0^2 D)^{-1}$. Here we have explicitly assumed diffusive particle motion; for non-diffusive random motion, the quantity $k_0^2 \langle \Delta r^2(t) \rangle/6$ may be substituted for t/τ. Note that eqn (16.26) represents an *incoherent* sum over light paths; that is, the contribution to the decay of $g_{(1)}(t)$ from each path is independent of all other paths. The validity of this assumption has been considered in a different context by several groups.[9, 10] They find that the coherent effects neglected here contribute terms that are smaller than the contribution from the coherent terms by a factor g^{-1}, where $g \approx (k_0 l^*)(k_0 L)$. Since $k_0 l^* \gg 1$ and $k_0 L \gg 1$ for nearly all cases of practical interest, contributions from coherent terms are negligible.

Equation (16.26) is the basis for the calculation of autocorrelation functions in diffusing-wave spectroscopy. It states that a light path of length s corresponds to a random walk of s/l^* steps and that such a path contributes, on average, $\exp(-2k_0^2 Dt)$ per step to the decay of the autocorrelation function. Furthermore, the characteristic decay time for a light path of length s is $\tau l^*/(2s)$, the

time it takes the total path length to change by $\approx \lambda$. Thus the decay time of long light paths will be relatively short and the decay time of short paths will be relatively long. Long paths decay relatively quickly, because each particle in the path must move only a small distance in order for the entire path length to change by one wavelength. Thus these long paths probe particle motion of length scales much less than one wavelength. This is one of the most unique and powerful features of DWS. Although eqn (16.26) has been derived from the simple case of uncorrelated colloidal particles, it can be generalized to highly correlated systems, provided that the correlation length and transport mean free path remain small compared with the size of the system. This generalization is discussed in Section 16.2.5.

16.2.3.2 *Calculation of $P(s)$ and $g_{(1)}(t)$.* The path length distribution $P(s)$ depends on the size and shape of the sample, the place where light enters the sample, and the point from which the outgoing light is collected. For example, consider the case of light incident at a point r_{in} on the face of a slab of thickness L and collected from a point r_{out} on the opposite face, as shown in Fig. 16.1. The detected light must 'diffuse' an end-to-end distance L before leaving at the point r_{out}. Thus nearly all the photons leaving the sample will have scattered $\approx (L/l^*)^2(l^*/l)$ times, corresponding to $n_c \approx (L/l^*)^2$ random walk steps, and will have travelled a total distance of $s_c \sim n_c l^*$. Since all photons scatter approximately the same number of times, $g_{(1)}(t)$ will decay nearly exponentially (assuming diffusive particle motion). In contrast, consider the case of light incident over a broad area on the face of a very thick slab and collected from 6)a point near the centre of the illuminated area on the same face, as shown in Fig. 16.4. Some photons will enter the sample and scatter only a few times before leaving and being collected; other photons will scatter many times before being collected. Thus there will be a very broad distribution of photon path lengths through the sample and a correspondingly broad distribution of decay times. For this geometry, we expect that $g_{(1)}(t)$ will be highly non-exponential. Thus it is clear that $P(s)$ must be determined for each experimental configuration.

We illustrate our method of calculating $P(s)$ by considering a simple thought experiment. An instantaneous pulse of light is incident over some area of the sample. Light entering the sample is multiply scattered and executes a random walk until it escapes. There will be some delay after the initial pulse before any light is detected, because of the finite transit time between the entrance point r_{in} and exit point r_{out}. The light intensity will rise to some maximum and then fall back to zero at long times, when all the photons have left the sample. Photons arriving at time t after the incident pulse will have travelled a distance $s = vt$ through the sample, where v is the average speed of light within the medium.[21] The flux $J_{out}(r_{out}, t)$ of photons arriving at the point r_{out} will be directly proportional to the fraction of photons that travel a distance $s = vt$, that is, to $P(s)$. For length scales greater than the transport mean free path, the
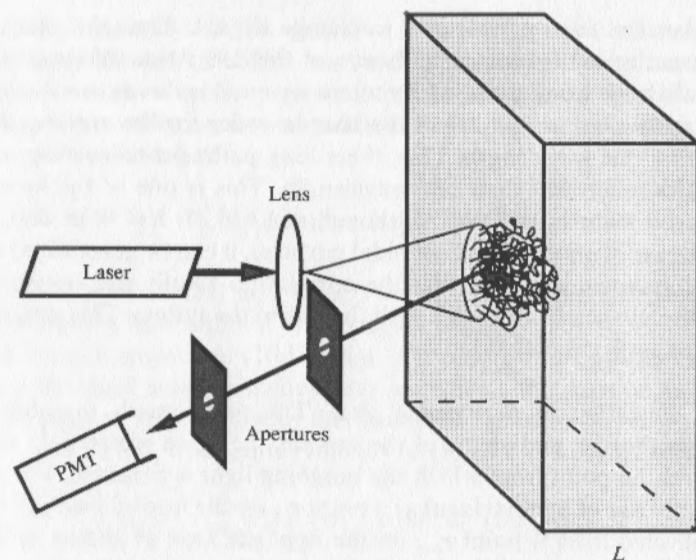
FIG. 16.4. Typical optical arrangement for DWS in the backscattering geometry, showing the large number of possible diffusion paths that the photons can follow. The laser beam is spread by a lens so that light in incident over a wide area on the left face of the sample; light is collected from a point near the centre of the illuminated area on the same face. The apertures define the point from which approximately one speckle of the scattered light is collected. Only those paths collected by the light detector (PMT) are shown. Both long and short paths will be collected in this geometry.

transport of light is accurately described by the diffusion equation

$$\frac{\partial U}{\partial t} = D_l \nabla^2 U, \tag{16.27}$$

where U is the energy density of light (or number of photons per unit volume) in the sample, and $D_l = vl*/3$ is the diffusion coefficient of light. Thus we can exploit the diffusive nature of light transport in highly scattering media to calculate $J_{out}(r_{out}, t)$ by solving the diffusion equation for light and thereby obtain $P(s)$.

To calculate $P(s)$, we consider an instantaneous light pulse propagating along the z-direction which is incident at $z = 0$ on a planar sample of thickness L. Since the light is randomized within the sample over a distance comparable with $l*$, we describe the incident pulse as an instantaneous source of *diffusing* light a distance $z_0 \approx l*$ inside the sample. Thus the initial condition is

$$U(z, t = 0) = U_0 \delta(z - z_0, t). \tag{16.28}$$

In addition to this initial condition, we must also specify the boundary conditions for the diffusing light. These are obtained by requiring that for $t > 0$

the net flux of diffusing light *into* the sample is zero.[1,5] The result is the boundary condition

$$U + \frac{2}{3}l*\hat{n}\cdot\nabla U = 0, \tag{16.29}$$

where $\hat{n}$ is the unit normal vector directed out of the sample. An alternative boundary condition is sometimes used in which U is forced to be zero some *extrapolation length* outside the sample, usually taken to be $\frac{2}{3}l*$ or $0.7104l*$. This boundary condition gives results that are numerically very similar to results given by eqn (16.29). Another boundary condition that is sometimes used is a totally absorbing condition in which U is set equal to zero at the sample boundaries. The totally absorbing boundary condition is useful because it results in somewhat simpler calculations than the mixed boundary conditions of eqn (16.29). However, this boundary condition gives results which systematically differ by approximately 10 to 20 per cent from the results given by the mixed boundary conditions. Furthermore, the predictions resulting from the mixed boundary conditions are in much better agreement with measurements than are those given by the absorbing boundary conditions.[5] Thus, using the initial condition given in eqn (16.28) and the boundary conditions given in eqn (16.29), we can solve the diffusion equation, eqn (16.27), for any particular experimental geometry and obtain a solution for $U(r)$ valid for all points within the sample. From this solution, we can calculate the time-dependent flux of light emerging from the sample at the exit point, r_{out}, using Fick's law.[11] Since all light emerging from the sample at time t has travelled a distance $s = vt$, the fraction of light, $P(s)$, that travels a distance s through the same is simply proportional to the flux emerging at time $t = s/v$. Thus $P(s)$ is given by

$$P(s) \propto |J_{out}(r, t)|_{r_{out}} = D_l|\hat{n}\cdot\nabla U|_{r_{out}} = \frac{vU}{2}\bigg|_{r_{out}}. \tag{16.30}$$

Once an expression for $P(s)$ has been obtained for a given experimental geometry, eqn (16.27) can be used to determine $g_{(1)}(t)$.

The scheme described above for calculating $g_{(1)}(t)$ can be greatly simplified by exploiting the fact that eqn (16.26) is, with suitable definition of variables, the Laplace transform of $P(s)$. Thus, instead of solving the diffusion equation for light to obtain $P(s)$, we can solve the Laplace transform of the diffusion equation and obtain $g_{(1)}(t)$ directly without explicitly calculating $P(s)$. To facilitate this transformation, we introduce a change of variables into the diffusion equation and let $t = s/v$. Thus eqn (16.27) becomes

$$\nabla^2 U - \frac{3}{l*}\frac{\partial U}{\partial s} = 0. \tag{16.31}$$

Multiplying both sides by $\exp(-ps)$ and integrating over all s, we obtain the

Laplace transform of the diffusion equation:

$$\nabla^2 \bar{U} - \frac{3p}{l^*}\bar{U} = -\frac{3p}{l^*}U_{00}(r), \qquad (16.32)$$

where $\bar{U} \equiv \bar{U}(r, p)$ is the Laplace transform of $U(r, s)$,

$$\bar{U}(r, p) \equiv \int_0^\infty e^{-ps}U(r, s)\,ds, \qquad (16.23)$$

and $U_{00}(r) = \lim_{t \to 0} U_0\delta(z - z_0, t)$. In solving this equation, we must also use the Laplace transform of the boundary conditions, eqn (16.29):

$$\bar{U} + \tfrac{2}{3}l^*\hat{n}\cdot\nabla\bar{U} = 0. \qquad (16.34)$$

These equations can then be solved using Green's function techniques to obtain $\bar{U}(r, p)$, as discussed by Carslaw and Jaeger.[11] Carslaw and Jaeger also give explicit expressions for $\bar{U}(r, p)$ for many geometries of experimental interest. Taking the Laplace transform of eqn (16.30), we can relate this solution, $\bar{U}(r, p)$, to the Laplace transform of $P(s)$:

$$\bar{P}(p) \equiv \int_0^\infty P(s)\,e^{-ps}\,ds \propto \frac{v}{2}\,\bar{U}(r, p)\Big|_{r_{out}}. \qquad (16.35)$$

We note that the Laplace transform of $P(s)$ in eqn (16.35) has exactly the same form as the general expression for $g_{(1)}(t)$ given in eqn (16.26). Thus we obtain

$$g_{(1)}(t) = \frac{\bar{U}(r, p)|_{r_{out}}}{\bar{U}(r, 0)|_{r_{out}}}, \qquad (16.36)$$

where we have made the identification $p = 2t/(\tau l^*)$ and $\bar{U}(p)$ has been normalized so that $g_{(1)}(0) = 1$.

16.2.3.3 Transmission.

A geometry commonly used in DWS experiments is the transmission geometry.[4, 5] The transmission geometry is simpler to interpret than the backscattering geometry because all paths through the sample are long compared with l^* and are therefore accurately described within the photon diffusion approximation. Furthermore, the transmission geometry allows one to probe motion over length scales much shorter than the wavelength of light and thereby takes advantage of one of the most appealing and useful features of DWS. In a transmission experiment, light is incident on one side of a sample of thickness L and is detected on the opposite side. The incident light can either be focused to a point or expanded to cover some or all of the incident face. In either case we take the source of diffusing intensity to be a distance z_0 inside the sample where we expect that $z_0 \approx l^*$, the distance over which the incident light is randomized. The simplest case to consider is that of uniform illumination of the incident face, which we take to be at $z = 0$. In this case the initial condition

is given by an instantaneous planar source at $z = z_0$, so that $U(x, y, z, t) = U_0\delta(z - z_0, t)$.

The solution to the diffusion equation for this geometry and these initial conditions is given in §14.3 of Carslaw and Jaeger.[11] Using Laplace transform techniques, they obtain

$$\bar{U} = \frac{1}{2D_1\alpha}e^{-q|z-z_0|} + A\sinh(\alpha z) + B\cosh(\alpha z), \qquad (16.37)$$

where $\alpha^2 \equiv 3p/l^* = 6t/(\tau l^{*2})$ and $D_1 = vl^*/3$. The constants A and B are chosen to satisfy the boundary conditions obtained from eqn (16.29),

$$\bar{U} - \tfrac{2}{3}l^*\frac{d\bar{U}}{dz} = 0 \quad \text{at } z = 0, \qquad (16.38a)$$

$$\bar{U} + \tfrac{2}{3}l^*\frac{d\bar{U}}{dz} = 0 \quad \text{at } z = L. \qquad (16.38b)$$

Solving for $\bar{U}(p, z)$ and applying eqn (16.36) at $z_{out} = L$, we obtain

$$g_{(1)}(t) = \frac{\dfrac{L/l^* + 4/3}{z_0/l^* + 2/3}\left\{\sinh\left[\dfrac{z_0}{l^*}\sqrt{\dfrac{6t}{\tau}}\right] + \dfrac{2}{3}\sqrt{\dfrac{6t}{\tau}}\cosh\left[\dfrac{z_0}{l^*}\sqrt{\dfrac{6t}{\tau}}\right]\right\}}{\left(1 + \dfrac{8t}{3\tau}\right)\sinh\left[\dfrac{L}{l^*}\sqrt{\dfrac{6t}{\tau}}\right] + \dfrac{4}{3}\sqrt{\dfrac{6t}{\tau}}\cosh\left[\dfrac{L}{l^*}\sqrt{\dfrac{6t}{\tau}}\right]} \qquad (16.39a)$$

$$\approx \frac{\left(\dfrac{L}{l^*} + \dfrac{4}{3}\right)\sqrt{\dfrac{6t}{\tau}}}{\left(1 + \dfrac{8t}{3\tau}\right)\sinh\left[\dfrac{L}{l^*}\sqrt{\dfrac{6t}{\tau}}\right] + \dfrac{4}{3}\sqrt{\dfrac{6t}{\tau}}\cosh\left[\dfrac{L}{l^*}\sqrt{\dfrac{6t}{\tau}}\right]}, \qquad (16.39b)$$

where the second expression holds for $t \ll \tau$. While the analytic form of these expressions appears to be complicated, the correlation functions are very nearly exponential in time, with a slight upward curvature when plotted on a log–linear graph. The characteristic decay time for eqn (16.39) is $\tau(l^*/L)^2$. Since DWS experiments are usually performed with $(l^*/L) \ll 1$, eqn (16.39b) is generally a good approximation for $g_{(1)}(t)$.

Another transmission geometry of interest is that of a point source. The advantages of using a point source configuration instead of an extended plane wave source are that the intensity of the light collected in transmission is greater for a given total power of the incident light, and that less light will leak out of the sides of a sample of finite lateral extent. The disadvantage is that the local energy density at the point where the light is incident may be so high as to cause significant local heating of a sample exhibiting even only a modest degree of absorption. Thus in some cases it may be desirable to use a source that has a finite diameter not much greater than the sample thickness. Hence we consider

below both cases of a point source and a source with a Gaussian profile of arbitrary finite width. First we consider the point source.

For the point source, we take the instantaneous source of diffusing intensity to be at (x_0, y_0, z_0), so that $U(x, y, z, t) = U_0 \delta(R, z - z_0, t)$, where $R^2 = (x - x_0)^2 + (y - y_0)^2$. The detected light is collected from the multiply-scattered light emerging from the sample at $(x, y, z) = (0, 0, L)$. The Laplace transform solution for this geometry is given in §14.10 of Carslaw and Jaeger:[11]

$$\bar{U} = \frac{1}{4\pi D_1} \int_0^\infty \frac{\xi J(\xi R)}{\eta} [e^{-\eta|z - z_0|} + A \sinh(\eta z) + B \cosh(\eta(L - z))] \, d\xi, \quad (16.40)$$

where $\eta = \sqrt{\xi^2 + \alpha^2}$, and $\alpha^2 \equiv 3p/l^* = 6t/(\tau l^{*2})$. Once again the coefficients A and B are obtained by applying the boundary conditions given in eqn (16.38). Thus we solve for $\bar{U}$ and use eqn (16.36) to obtain

$$g_{(1)}(t) = C \int_Q^\infty J_0 \left(\frac{R}{L} \sqrt{\xi^2 - Q^2} \right) D(\xi, \varepsilon, \zeta) \xi \, e^{-(1 - \zeta)\xi} \, d\xi, \quad (16.41)$$

where $Q \equiv (L/l^*)\sqrt{6t/\tau}$, $\varepsilon \equiv 2l^*/(3L)$, $\zeta \equiv z_0/L$, and C is a normalization constant chosen so that $g_{(1)}(0) = 1$. The function $D(\xi, \varepsilon, \zeta)$ is given by

$$D(\xi, \varepsilon, \zeta) = \frac{2\varepsilon[(1 + \varepsilon\xi) - (1 - \varepsilon\xi) e^{-2\zeta\xi}]}{(1 + \varepsilon\xi)^2 - (1 - \varepsilon\xi)^2 e^{-2\xi}}. \quad (16.42)$$

Equation (16.41) can be used to obtain $g_{(1)}(t)$ for an incident beam with a Gaussian cross-section of arbitrary width which is on axis with the detector. In this case the instantaneous point source is taken to be

$$U(x, y, z, t) = U_0 \, e^{-4(x^2 + y^2)/d^2} \delta(z - z_0, t), \quad (16.43)$$

where d is the Gaussian beam diameter. The detected light is collected from the multiply-scattered light emerging from the sample at $(x, y, z) = (0, 0, L)$. The solution to this problem is obtained simply by integrating R in eqn (16.41) over the source distribution in eqn (16.43). By this procedure we obtain

$$g_{(1)}(t) = C' \int_Q^\infty e^{-(\xi^2 - Q^2)(\delta/4)^2} D(\xi, \varepsilon, \zeta) \xi \, e^{-(1 - \zeta)\xi} \, d\xi, \quad (16.44)$$

where $\delta \equiv d/L$ and C' is a normalization constant. If the beam diameter is much less than the thickness of the sample, i.e., $\delta = d/L \ll 1$, then eqn (16.44) reduces to that for a point source on axis with the detector, i.e., eqn (16.41) with $R = 0$.

All of the autocorrelation functions for the transmission geometry decay with a characteristic time of approximately $(l^*/L)^2 \tau$, reflecting the fact that there is a characteristic number of random-walk steps, $n_c \approx (L/l^*)^2$, and that the autocorrelation function decays, on average, $\exp(-2t/\tau)$ per step. This time-scale is set by the time it takes for the total length of a path to change by one wavelength or, equivalently, by the time it takes for the total phase of a

characteristic path to change by $\approx \pi$. We can estimate the distance an individual particles moves in a decay time from the total phase shift, $\Delta\phi \approx n_c \langle q^2 \rangle \langle r^2 \rangle \approx \pi$, which gives $\Delta r_{rms} \approx \lambda l^*/L$. Since $l^*/L \ll 1$, $\Delta r_{rms} \ll \lambda$, in DWS the motion of particles is probed over length scales that are much less than the wavelength of light. This is in contrast to conventional single-scattering DLS measurements in which particle motion is probed over length scales comparable with or longer than the wavelength of light. Moreover, in conventional DLS measurements the length scale over which motion is probed is adjusted by varying the scattering angle θ and thus changing the scattering vector q. In contrast, in DWS the length scale over which particle motion is proved is adjusted by changing the sample thickness L. However, the nature of the probe over different length scales is very different in DWS from that in DLS. In DLS, a single Fourier component of the particle motion is probed; this is set by the value of q. In DWS, the scattering reflects an average over all q, weighted by the scattering form factor (see the discussion following eqn (16.20)). Furthermore, since the number of scattering events is large, there is no appreciable angular dependence of the fluctuations in the transmitted light.

A schematic diagram of the experimental apparatus for a transmission measurement with uniform illumination is shown in Fig. 16.5. Autocorrelation functions measured in transmission are shown in Fig. 16.6. The data shown are for an aqueous suspension of 0.605 μm diameter polystyrene spheres at a volume fraction of spheres $\phi = 0.012$, with $L = 0.10$ cm. The two data sets correspond to essentially uniform illumination (lower curve) of the incident face and what amounts to a point source (upper curve). Uniform illumination is attained by expanding the incident laser beam so that it uniformly illuminates an area much wider than the sample thickness; for the lower curve in Fig. 16.6, the width of the illuminated area is approximately 1 cm. Point source illumination is attained for focusing the laser to a point much narrower than the sample
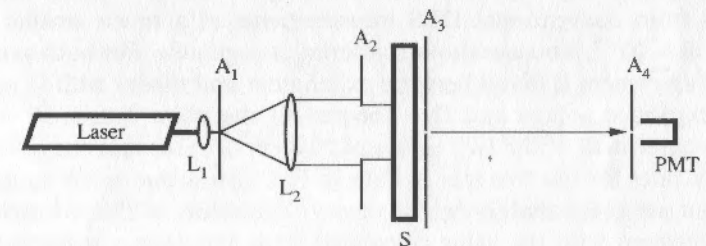

FIG. 16.5. Experimental set-up for transmission measurements. The laser beam is expanded by lens L_1, passes through aperture A_1 which serves as a spatial filter, and is collimated by lens L_2. The aperture A_2 selects the central constant-intensity part of the expanded beam which impinges on the sample S. Apertures A_3 and A_4 define roughly one speckle for detection by photomultiplier tube PMT. The output of the photomultiplier tube is passed to a digital correlator. The aperture A_1 and lens L_2 can be omitted without adversely affecting the signal in most cases.
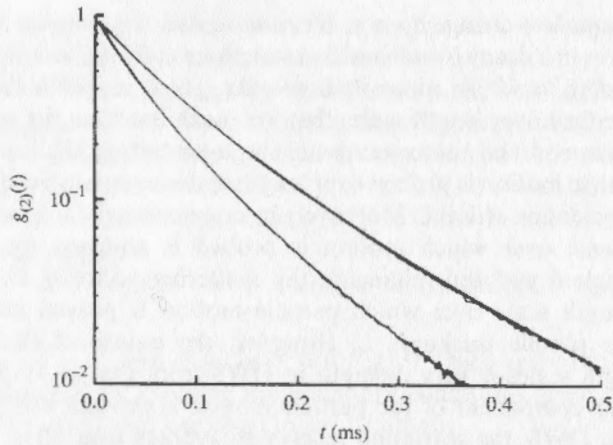
FIG. 16.6. Transmission measurements. The smooth lines through the data are fits to the data using eqns (16.39a) and (16.41) with $l^* = 167$ μm for the expanded source and $l^* = 166$ μm for the point source ($R = 0$).

thickness; for the upper curve in Fig. 16.6, the width of the laser beam is less than 50 μm. While both data sets exhibit nearly exponential behaviour, the data from the expanded source decay more rapidly than the data from the point source. This difference results from the fact that the extended source geometry has a relatively larger contribution from long paths than the point source geometry and therefore decays more rapidly. The smooth curves through the data are fits using Eqns (16.39a) and (16.41) with $z_0 = l^*$.[5] We note that the numerical values of these expressions are insensitive to the exact choice of the value of z_0, since $L \gg z_0$; a different choice of z_0 would affect only the first few steps in a random walk that consists of a large number of steps. The fits were obtained by allowing l^* to vary and by setting $\tau = (Dk_0^2)^{-1} = 4.52$ ms, with D obtained from conventional DLS measurements at a much smaller volume fraction, $\phi = 10^{-5}$, where multiple scattering is negligible. For both geometries, excellent agreement is found between experiment and theory with $l^* = 167$ μm for the expanded source and $l^* = 166$ μm for the point source ($R = 0$). The excellent agreement of the two values of l^* demonstrates that the difference in the decay rates for the two sets of data in Fig. 16.6 is due solely to geometric effects that are accounted for by the theory. The values of l^* are in reasonably good agreement with the value calculated from Mie theory using eqn (16.8): $l^* = 180$ μm.

16.2.3.4 *Backscattering.* Another geometry commonly used in DWS experiments is the backscattering geometry.[3–5] This geometry is very convenient because it requires access to a sample from only one side. This can be particularly useful in industrial process-monitoring applications where production

constraints limit access to the sample. Another advantage of the backscattering geometry is that it does not require independent knowledge of the transport mean free path in order to interpret the autocorrelation function. From a more fundamental viewpoint, the backscattering geometry is both useful and often difficult to interpret because it probes many length scales at once. This ability to probe many length scales at once can in principle reveal a wealth of information about particle motion. However, because backscattering involves a significant number of light paths whose length is comparable with l^*, the diffusion approximation must be used with caution in describing light transport for this geometry.

In a backscattering experiment, the laser beam is usually expanded so that it uniformly illuminates an area of the incident face that is much wider than l^* (see Fig. 16.4). Light is collected from a very small area near the centre of the illuminated area. This ensures that the shape of the measured autocorrelation function is insensitive to the size of the illuminated area and to the precise position of the detected light within that area. The thickness of the sample is L. As in the case of the transmission geometry, we again take the incident face to be at $z = 0$ and the source of diffusing intensity to be a distance z_0 which we expect to be of order l^* inside the sample. In contrast to transmission, in backscattering the distribution of path lengths, and in particular the relative weighting of *short* path lengths, will depend critically on the exact choice of the value of z_0. The consequences of choosing different values for z_0 are discussed in Section 16.2.4.

The initial condition is once again given by an instantaneous planar source at $z = z_0$, so that $U(x, y, z, t) = U_0\delta(z - z_0, t)$. The solution for $\bar{U}(p, z)$ is again given by eqn (16.37) and the constants are given by eqn (16.38b). Thus we use the same solution for $\bar{U}(p, z)$ obtained for the transmission geometry with an extended source but now apply eqn (16.36) at the incident face, $z_{\text{out}} = 0$. This gives

$$g_{(1)}(t) = \frac{\sinh\left[\sqrt{\frac{6t}{\tau}}\left(\frac{L}{l^*} - \frac{z_0}{l^*}\right)\right] + \frac{2}{3}\sqrt{\frac{6t}{\tau}}\cosh\left[\sqrt{\frac{6t}{\tau}}\left(\frac{L}{l^*} - \frac{z_0}{l^*}\right)\right]}{\left(1 + \frac{8t}{3\tau}\right)\sinh\left[\frac{L}{l^*}\sqrt{\frac{6t}{\tau}}\right] + \frac{4}{3}\sqrt{\frac{6t}{\tau}}\cosh\left[\frac{L}{l^*}\sqrt{\frac{6t}{\tau}}\right]}, \quad (16.45)$$

For a sample of infinite thickness, this expression simplifies to give

$$g_{(1)}(t) = \frac{\exp\left[-\frac{z_0}{l^*}\sqrt{\frac{6t}{\tau}}\right]}{1 + \frac{2}{3}\sqrt{\frac{6t}{\tau}}}. \quad (16.46)$$

The stretched exponential form of eqn (16.46) reflects the wide distribution of

decay times, which in turn results from the wide distribution of path lengths inherent in the backscattering geometry. Long paths, which decay quickly and probe relatively short length-scale motion, contribute to the initial delay of the autocorrelation function. In fact, the initial slope of $g_{(1)}(t)$ in eqn (16.46) is infinite, reflecting the contribution of infinitely long paths. At longer times, after the contributions from long paths have decayed away, the decay of the autocorrelation function comes from short paths and probes relatively long length-scale motion. Although it is tempting to replace $6t/\tau$ in eqn (16.46) with $k_0^2 \langle \Delta r^2(t) \rangle$ and use backscattering measurements to probe $\langle \Delta r^2(t) \rangle$ over the full range of decay times, such an analysis of the data cannot be correct, except for the initial decay. This is because the diffusion approximation and central limit theorem used in arriving at this result are valid only for long paths, and break down for short paths.

A schematic diagram of the experimental set-up for a backscattering measurement is shown in Fig. 16.7. The sample was illuminated by a 1 cm diameter beam and collected at an angle of $\approx 175°$ with respect to the incident direction. The apertures ensure that a single speckle of light is collected from a spot approximately 50 μm in diameter from the centre of the illuminated area. An autocorrelation function measured in backscattering is shown in Fig. 16.8. Data are shown for an aqueous suspension of 0.412 μm diameter spheres at a volume fraction $\phi = 0.05$. The data are plotted logarithmically as a function of $\sqrt{t}$ as suggested by the theoretical form given in eqn (16.46). While the data are fitted very well by eqn (16.46), they are equally well fitted by the simpler form

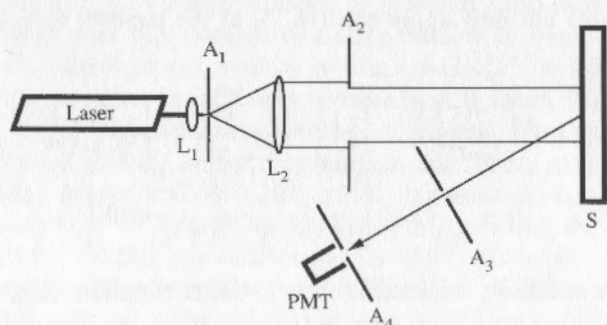$$g_{(1)}(t) = e^{-\gamma\sqrt{6t/\tau}}, \tag{16.47}$$

FIG. 16.7. Experimental set-up for backscattering measurements. The laser beam is expanded by lens L_1, passes through aperture A_1 which serves as a spatial filter, and is collimated by lens L_2. The aperture A_2 selects the central constant-intensity part of the expanded beam which impinges on the same S. Apertures A_3 and A_4 select a spot from the centre of the illuminated area and define roughly one speckle for detection by a photomultiplier tube PMT. The output of the photomultiplier tube is passed to a digital correlator.
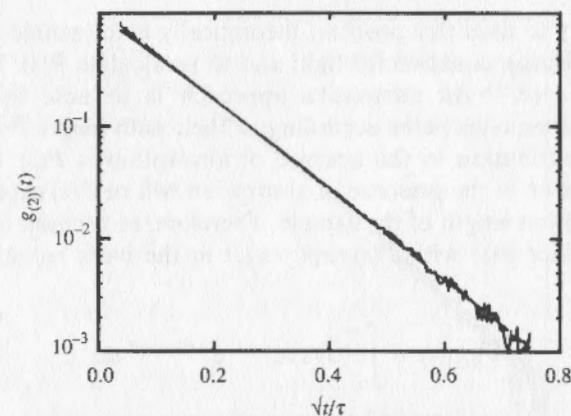
FIG. 16.8. Backscattering measurements from an aqueous suspension of polystyrene spheres at a volume fraction $\phi = 0.05$. The data are plotted logarithmically as a function of the square root of the reduced time. The smooth line through the data represents fits to the data using eqns (16.46) and (16.47), which, within the resolution of the figure, are indistinguishable.

where $\gamma = \langle z_0 \rangle + \frac{2}{3}$ is chosen to be consistent with the initial decay given by eqn (16.46). Although the qualitative behaviour exhibited by the data in Fig. 16.8 is generally observed in backscattering measurements, there are systematic variations in the data which depend on the particle size and the polarization states of the incident and collected light. For example, the value of γ is observed experimentally to vary between 1.5 and 2.7 as particle size and polarization states are varied.[12] Furthermore, when plotted logarithmically vs. $\sqrt{t}$, the data can exhibit either slight downward or upward curvature or no curvature at all, depending on system parameters.[12, 13] These variations in the value of γ and the shape of $g_{(1)}(t)$ have their origin in the different contributions of short non-diffusive light paths which occur under different experimental conditions and are an important limitation of the photon diffusion approximation. These limitations are more fully explored in Section 16.2.4.

16.2.3.5 *Absorption.* In any DWS experiment there will always be some absorption. The qualitative effects of absorption on an experiment are twofold. First, if the absorption is very strong and the incident laser intensity is high, absorption of the incident radiation may locally heat the sample. This effect can usually be avoided by spreading out the incident beam over a sufficiently large area for local heating to be insignificant. If necessary, the sample may also be put in contact with a heat sink, such as a water bath, in order to minimize heating.

The second effect of absorption is that it alters the distribution of light path lengths, $P(s)$, and in particular attenuates long paths more strongly than short

paths. One way to treat this problem theoretically is to include an absorption term in the diffusion equation for light and to recalculate $P(s)$. This approach is commonly used.[1] An alternative approach is to note that absorption exponentially attenuates paths according to their path length.[5, 14] Thus if the path length distribution in the absence of absorption is $P(s)$, then the path length distribution in the presence of absorption will be $P(s)\exp(-s/l_a)$, where l_a is the absorption length of the sample. Therefore, to account for absorption, we simply replace $P(s)$ with $P(s)\exp(-s/l_a)$ in the basic equation for $g_{(1)}(t)$, eqn (16.26):

$$g_{(1)}(t) = \int_0^\infty P(s)\, e^{-s/l_a}\, e^{-(2t/\tau)s/l^*}\, ds \qquad (16.48a)$$

$$= \int_0^\infty P(s)\, e^{-(2t/\tau + l^*/l_a)s/l^*}\, ds. \qquad (16.48b)$$

Since both exponential terms in eqn (16.48a) are linear in s, the effect of absorption on $g_{(1)}(t)$ is mathematically the same as a shift in the time axis. Thus all the results that we derived previously for $g_{(1)}(t)$ can be adapted to account for absorption simply by making the substitution

$$\frac{t}{\tau} \rightarrow \frac{t}{\tau} + \frac{l^*}{2l_a}. \qquad (16.49)$$

For example, the autocorrelation function given in eqn (16.47) for backscattering becomes

$$g_{(1)}(t) = e^{-\gamma\sqrt{6t/\tau + 3l^*/l_a}}. \qquad (16.50)$$

The effect of absorption on correlation functions obtained in the backscattering geometry is illustrated in Fig. 16.9. Absorption in the samples was adjusted by adding known amounts of methyl red, an absorbing dye. The absorption lengths, l_a, were independently measured to be 4.87 mm for the upper curve and 2.53 mm for the lower curve. Physically, the effect of absorption is to cut off the longest paths. This effect is evident in the data in Fig. 16.9 in the rounding of the correlation functions at early times, showing that the longest, fastest decaying paths are the most affected by absorption. Furthermore, the effect becomes more pronounced as the absorption becomes stronger. The value of γ was taken from measurements without dye, so that there are no adjustable parameters in the fits to the data in Fig. 16.9. The excellent agreement between the theory and the data confirms the validity of the general expression given in eqn (16.48b).

Absorption can also have significant effects in the transmission geometry. By cutting off the longest paths, absorption will tend to slow the decay of the autocorrelation function. Since the decay of the autocorrelation function in the transmission geometry is dominated by paths of a single characteristic length,
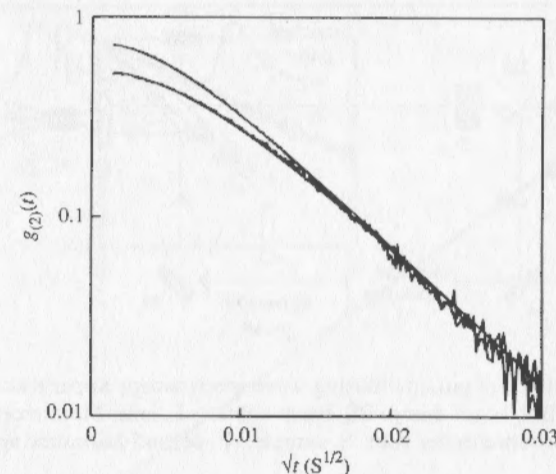
FIG. 16.9. Intensity autocorrelation functions for samples with known amounts of absorbing dye in aqueous solution. The rounding at early times illustrates the effect of absorption, which is to attenuate the contribution of the longest, fastest-decaying light paths. The rounding at early times is most pronounced for the sample with the most absorption.

$s_c \approx L^2/l^*$, the absorption length must be comparable with s_c in order to slow the decay dramatically. In this case, however, the most significant effect of absorption will be a strong attentuation of the transmitted light, which may be large enough to reduce the signal to an unusable level.

16.2.3.6 *Pulsed diffusing-wave spectroscopy*.   In the preceding sections we have emphasized the need to calculate the distribution of path lengths, $P(s)$, through a sample in order to obtain an expression for $g_{(1)}(t)$. However, alternative approaches are available. For example, there are several schemes for directly measuring the path length distribution, using fast optical pulse techniques.[15–17] In principle, $g_{(1)}(t)$ could be calculated from such measurements of $P(s)$ using eqn (16.26), although such a scheme has not been pursued experimentally. However, another scheme for directly measuring the temporal autocorrelation function from paths of a *single length* has been developed using non-linear optical gating techniques.[18] With this technique, it is not necessary to know $P(s)$. Instead, one measures the path-dependent autocorrelation function, $g_{(1)}^s(t)$, for paths of a known specified length s. Thus $g_{(1)}^s(t)$ is a single-path-length exponential decay function which appears in eqn (16.26):

$$g_{(1)}^s(t) = \exp[-(2t/\tau)s/l^*]. \qquad (16.51)$$

The measurement of $g_{(1)}^s(t)$ employs very short laser pulses and is called pulsed diffusing-wave spectroscopy (PDWS).[18]
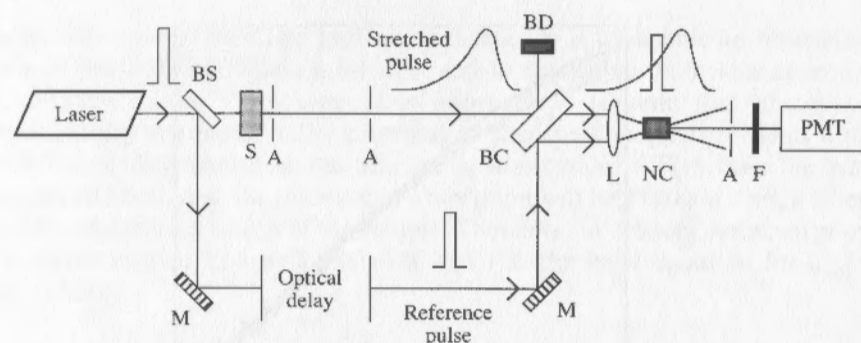
FIG. 16.10. Schematic of pulsed diffusing-wave spectroscopy apparatus: A, aperture; BC, beam combiner; BD, beam dump; BS, beam splitter; L, lens; M, mirror; NC, non-linear crystal; PMT, photomultiplier tube; S, sample; sF, second-harmonic spectral filter.

The experimental set-up and basic ideas of PDWS are illustrated in Fig. 16.10.[18] The laser used in a PDWS experiment emits a pulse train (≈ 100 MHz) of identical, short light pulses (20–90 ps) which are divided with a beamsplitter between the sample and a reference beam. The temporal width of a light pulse emerging from the sample is considerably longer than the incident pulse because of the distribution of path lengths, and also transit times, through the sample. In fact the temporal shape of the average intensity profile, $\bar{I}(t)$, is the same as $P(s)$. A portion of the multiply-scattered output light is recombined in a frequency-doubling crystal with a time-delayed reference pulse from the same laser; a second harmonic pulse train is produced when the two input fields non-linearly mix. Since the sample pulse is broadened by the multiple scattering, the short reference beam gates a small portion of the broad output pulse from the sample. If s' is the difference in the path length between the reference and sample arms with the sample removed, then each pulse within the combined second-harmonic pulse train will have a field $E(2\omega, t)$ proportional to the reference field, $E_R(t)$, and the path-dependent scattered field $E_0(t, s')$. Since fluctuations in the reference field are negligible, $E_R(t) = E_R$, and

$$E(2\omega, t) = E_R E_0(t, s'). \qquad (16.52)$$

The second harmonic electric field experiences the same fluctuations due to particle motion in the sample as does the scattered electric field for a single path length. For almost all cases of experimental significance, the time-scale of the fluctuations in the phase of the scattered light is much longer than the last pulse-train repetition rate. In this case, the graininess of the sample process is unimportant, and the autocorrelation function of the second-harmonic photons is

$$g_{(1)}(2\omega, t) = \frac{\langle E_0(t, s) E_0(t, 0)\rangle}{\langle |E_0|^2\rangle} = g^s_{(1)}(t), \qquad (16.53)$$
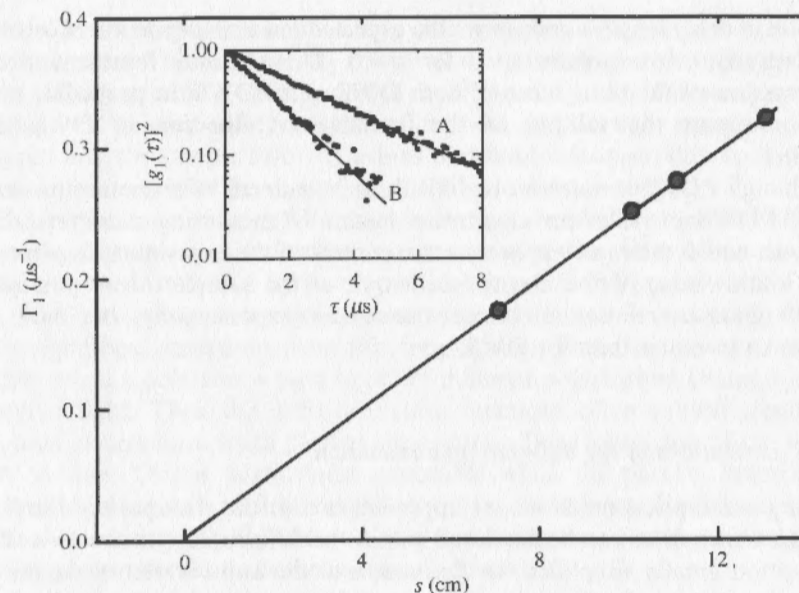
FIG. 16.11. Temporal decay rate, Γ_1, vs. path length s for the single-path-length intensity autocorrelation functions obtained in pulsed diffusing-wave spectroscopy measurements; Γ_1 is linear in s and passes through the origin, confirming the basic equations of DWS. Inset. Single-path-length intensity autocorrelation functions, $[g^s_{(1)}(t, s)]^2$, at delays, s, of (A) 7 cm, (B) 13 cm.

where $s = s'$. By varying the path length difference, s', between the sample and reference arms, the single-path correlation function can be measured for arbitrary s. Since only one path length is sampled at a time, we expect an exponential decay of the autocorrelation function. According to eqn (16.51), the rate of decay is given by $\Gamma_1 = 2s/(l^*\tau)$ and therefore should be proportional to s.

An important additional feature of this photon gating scheme is that the average second harmonic intensity, $\bar{I}(t)$, is proportional to $P(s)$. Thus $P(s)$ can be directly measured using the same PDWS apparatus. Since $P(s)$ is a sensitive function of l^* and l_a, a PDWS experiment can measure both l^* and l_a by fitting the measured $P(s)$ to predictions of photon diffusion theory, as outlined in Section 16.2.3.2.

Results from a series of PDWS measurements are shown in Fig. 16.11,[18] the inset which shows measurements of path-dependent autocorrelation functions obtained in a transmission geometry. A sample consisting of 0.46 μm diameter polystyrene spheres in water was used. The volume fraction of spheres was $\phi = 0.3$ and the sample thickness was $L = 0.2$ cm. The inset shows data taken at two different delays, $s = 7$ cm and $s = 13$ cm. As expected, the curves decay exponentially, in contrast to DWS. The decay rate, Γ_1, is plotted as a

function of delay length s and shows the expected linear dependence. Moreover, the decay rate extrapolates to 0 for $s = 0$. These results represent strong confirmation of the basic ideas of both DWS and PDWS; in particular these results support the validity of the fundamental equation of DWS, eqn (16.26).

Although PDWS is much more difficult to instrument than continuous-wave DWS, PDWS provides an alternative means of measuring autocorrelation functions which does not require precise control of the experimental geometry or any knowledge of the absorption length of the sample. Moreover, since PDWS gives correlation functions that decay exponentially, the data are simpler to interpret than for DWS.

16.2.4 *Limitations of the diffusion approximation*

The key assumption made in our approach is that the transport of the light through the medium can be described within the diffusion approximation. This assumption greatly simplifies our derivation of the autocorrelation functions. However, this is clearly only an approximation for describing the light transport, and in some instances it breaks down. The most important situation in which it fails is in the treatment of backscattered light. Light that is backscattered from a highly multiple-scattering sample contains a significant fraction that has been scattered only a few times. In fact, most of the light that is incident on the face of the sample never penetrates more than a distance l^* into the sample before it is scattered back. However, the diffusion approximation does not properly account for the behaviour at distances less than l^*. Thus, since so much of the backscattered light contributing to the decay of the autocorrelation function in backscattering results from photon paths of lengths less than l^*, the use of the diffusion approximation in deriving $g_{(1)}(t)$ does not properly account for the physics.

The problems with the use of the diffusion approximation are most apparent in the fact that we must include an additional factor, γ, in the expressions for the autocorrelation functions for backscattering. Within our derivation, this factor reflects the distance into the sample that light penetrates before it begins to diffuse. However, this is only an attempt to modify the description of the light scattering to force the diffusion approximation to describe the physics. This is not an accurate description, since the diffusion approximation cannot be used to account for paths less than l^*. The fact that it works at all is somewhat fortuitous. In our approach, we use the Laplace transform of the diffusion equation for light to obtain the autocorrelation functions. Taking the Laplace transform requires integration over all path lengths starting from $s = 0$. Clearly, the paths with $s = 0$ cannot be treated within the diffusion approximation. In addition, setting $s = 0$ in eqn (16.33) will result in paths that decay more slowly than even those with a single scattering event. Thus, to ensure a

physically meaningful minimum decay rate, we must introduce some cutoff in the decay rates. This is effectively the result of assuming that the light does not begin diffusing until it has traversed a distance z_0 into the sample. Thus although the physics underlying the assumptiom that the light must enter some distance into the sample before it begins to diffuse is suspect, the results are in better agreement with the data than one might otherwise expect.

The expression for $g_{(2)}(t)$ for backscattering derived within the diffusion approximation gives only limited agreement with the data. Most data are reasonably well described by an exponential decay in the square root of time, eqn (16.47). However, in many instances, closer examination of the data reveals some significant deviations from this simple form. These become particularly evident when a polarizer is used to detect different polarization channels of the scattered light. Then the autocorrelation functions often exhibit significant amounts of curvature when plotted logarithmically as a function of the square root of time. This is particularly noticeable when the parallel polarization channel is considered. In this channel there is a much larger contribution from paths that consists of only one or a very small number of scattering events. It is these paths that result in the curvature observed.

Improvement of the theoretical treatment for backscattering can come only from using a better approximation than the diffusion approximation. There have been several attempts to do this. To account directly for the discrete, as opposed to the continuum, nature of the very short scattering paths, computer simulations have been used.[19] These give good agreement with the functional form predicted in eqn (16.47).

A more analytical approach has been taken by Ackerson and co-workers.[20] They have generalized radiation theory to include the effects of correlations. Radiation transfer theory is a more exact treatment for the propagation of light through highly scattering media. It reduces to the diffusion approximation in suitable limits, but also is more accurate in describing the behaviour in regimes where a continuum approach is not adequate, such as for short paths. Radiation transfer theory simply follows the light through all its scatterimg events, in a statistical approximation. It neglects any interference effects within the medium, and thus treats only the propagating intensity, rather than the fields. It is for this reason that it must reduce to the diffusion approximation. However, since it follows the light through each scattering event, it is a better approach to use when discrete scattering events are important. Ackerson *et al.* have generalized radiation transfer theory by considering the transfer of correlations, as is important in calculating $g_{(2)}(t)$. They show that this approach is equivalent to the DWS approach for situations where long paths dominate, such as for transmission. For backscattering, where the discrete nature of the scattering events, the correlation transfer method seems to provide better agreement with the data without any *ad hoc* assumptions. This approach is still being developed but holds great promise for providing an improved theoretical treatment for DWS.

16.2.5 *Interactions and structure*

In the preceding sections we assumed that the particles that scatter light were non-interacting and completely uncorrelated. However, this is a good approximation only for dilute suspensions with relatively short-range interactions. More generally, particle positions and velocities will be correlated, especially in the dense suspensions for which DWS finds the widest application. Correlations between particles affect DWS in two ways. First, correlations between particle positions change the angular distribution of scattered light and therefore change the value of l^*. Since the length of a multiple-scattering path through a sample scales as $(l^*)^{-2}$ and the decay rate of such a path scales as $(l^*)^{-1}$, a change in the value of l^* can modify $g_{(1)}(t)$. However, since l^* appears simply as a multiplicative constant in the theory of DWS, a change in the value of l^* will simply multiply the time-scale of the decay of $g_{(1)}(t)$. Of greater importance is the fact that correlations between particle positions and velocities change the particle dynamics; these changes will be reflected in the time-dependence of $g_{(1)}(t)$. This is the second way in which correlations can affect DWS measurements.

To understand how correlations change l^*, we recall from eqn (16.21) that l^*/l can be written quite generally in terms of the mean square scattering vector:

$$\frac{l^*}{l} = \frac{2k_0^2}{\langle q^2 \rangle},\tag{16.54}$$

where $\langle\ \rangle$ denotes the angular average over all scattering angles, weighted by the scattering probability. For dilute systems, the scattering probability is simply the differential cross-section, or single-particle intensity form factor, which we write as $F(q)$. For correlated systems, we replace $F(q)$ by the full scattering function, $F(q)S(q)$, where $S(q)$ is the static stucture factor, Thus we obtain

$$\langle q^2 \rangle = \frac{\int_{4\pi} q^2 F(q)S(q)\, d\Omega}{\int_{4\pi} F(q)S(q)\, d\Omega},\tag{16.55}$$

or

$$\frac{l^*}{l} = \frac{2k_0^2 \int_{4\pi} F(q)S(q)\, d\Omega}{\int_{4\pi} q^2 F(q)S(q)\, d\Omega},\tag{16.56}$$

where $d\Omega$ is the solid angle element. Similarly, the mean free path is still given by eqn (16.7), but with the total cross-section given by

$$\sigma = \int_{4\pi} F(q)S(q)\, d\Omega.\tag{16.57}$$

In the limit of non-interacting particles, $S(q) = 1$ and this expression reduces to the usual result. Using eqns (16.7), (16.56), and (16.57), we can obtain a

general expression for l^* in interacting systems:[21]

$$l^* = k_0^6 a^4 \left(\pi\rho \int_0^{2k_0 a} I(x)x^3\, dx \right)^{-1},\tag{16.58}$$

where ρ is the number density of particles, a is the particle diameter, $x = qa$ is the dimensionless momentum transfer for a single scattering event, and $I(q)$ is the product of the form and structure factors $F(q)S(q)$.

The dynamic problem of DWS in interacting correlated systems has been treated carefully by MacKintish and John.[7] Here we follows a simple intuitive scheme suggested earlier by Maret and Wolf[3] and later extended.[13,22] In this approach we recall that for non-interacting, uncorrelated particles, the DWS autocorrelation is built up from the single-scattering result; we then follow the same procedure for interacting systems. In the single-scattering limit, light is scattered by concentration fluctuations, so that DLS measures the co-operative diffusion coefficient, $D_c(q)$, which is given by[8]

$$D_c(q) = D_0 \frac{H(q)}{S(q)},\tag{16.59}$$

where D_0 is the base Stokes–Einstein diffusion coefficient, $S(q)$ is the static structure factor of the colloidal suspension, and $H(q)$ is a q-dependent function describing the effect of hydrodynamic interactions between colloidal particles. In DLS, the initial decay of the autocorrelation function is given by

$$\langle E(0)E^*(t) \rangle = S(q)\, e^{-q^2 D_c(q)t}\tag{16.60a}$$

$$= S(q)\, e^{-q^2 D_0 [H(q)/S(q)]t}.\tag{16.60b}$$

We need to consider only the initial decay of the correlation function, as given by eqn (16.60b), because the large number of scattering events ensure that longer times, which lead to non-exponential decay in DLS, are never reached. Then we can view DWS in an interacting correlated system as a succession of isolated scattering events from volumes of spatial extent $\approx q^{-1}$ and separated by a mean free path l. Thus, for a large number of scattering events, n, the contribution to the decay of the autocorrelation function from paths of length $s = nl$ is given by the product of the single-scattering autocorrelation functions, averaged over all angles,

$$g_{(1)}^*(\tau) = \exp\left\{ -\left\langle q^2 D_0 \tau \frac{H(q)}{S(q)} \right\rangle n \right\}.\tag{16.61}$$

The angular average is weighted by the product of the particle form factor and

the structure factor, $F(q)S(q)$, i.e.,

$$n\left\langle q^2 D_0\tau \frac{H(q)}{S(q)}\right\rangle = nD_0\tau \frac{\int_{4\pi} q^2 \frac{H(q)}{S(q)} F(q)S(q)\,\mathrm{d}\Omega}{\int_{4\pi} F(q)S(q)\,\mathrm{d}\Omega} \qquad (16.62a)$$

$$= nD_0\tau \frac{\int_{4\pi} H(q)F(q)q^2\,\mathrm{d}\Omega}{\int_{4\pi} S(q)F(q)\,\mathrm{d}\Omega}, \qquad (16.62b)$$

To make use of the photon diffusion approximation, we must eliminate all explicit reference to n and l in our equations for the autocorrelation function. To this end, we express the total number of scattering events as $n = s/l = (s/l^*) \times (l^*/l)$. Using the expression for l^*/l in eqn (16.56), we obtain

$$n\left\langle q^2 D_0\tau \frac{H(q)}{S(q)}\right\rangle = 2k_0^2 D_0 t \frac{[H(q)]}{[S(q)]} \frac{s}{l^*}, \qquad (16.63)$$

where $[\ldots]$ denotes

$$[X(q)] = \frac{\int_{4\pi} X(q)F(q)q^2\,\mathrm{d}\Omega}{\int_{4\pi} F(q)q^2\,\mathrm{d}\Omega}. \qquad (16.64)$$

The full autocorrelation function is then obtained by integrating over all path lengths,

$$g_{(1)}(t) = \int_0^\infty P(s) \exp\left(-2k_0^2 D_0 t \frac{[H(q)]}{[S(q)]} \frac{s}{l^*}\right) \mathrm{d}s. \qquad (16.65)$$

The only length scale appearing in eqn (16.65) for the transport of photons is l^*. Moreover, eqn (16.65) has exactly the same form as eqn (16.26) if we identify τ with a q-averaged diffusion coefficient so that $\tau = (D_{av}k_0^2)^{-1}$ and

$$D_{av} = D_0 \frac{[H(q)]}{[S(q)]}. \qquad (16.66)$$

With this definition, we can now adapt the results for the $g_{(1)}(t)$ derived previously for uncorrelated particles and apply them to correlated interacting systems for the various scattering geometries.

Equation (16.65) has been tested experimentally for the backscattering geometry[13] and for the transmission geometry.[22] In both sets of experiments, monodisperse suspensions of polystyrene spheres were used, with volume fractions ranging from 0.01 to 0.5. Although the polystyrene spheres used were charged, the charges were highly screened so that the interparticle potential was well approximated by a hard-sphere interaction. Thus theoretical expressions

for the hydrodynamic interaction function, $H(q)$, and the Percus–Yevick expression for the static structure factor, $S(q)$, could be used to test the validity of eqn (16.65). Good agreement between experiment and theory was obtained in both instances.

In the limit of particles somewhat larger than the wavelength of light, the diffusion coefficient measured with DWS, eqn (16.66), takes on a particular simple and useful form. In this context, it is convenient to rewrite eqn (16.66) as

$$D_{av} = D_s \frac{[h(q)]}{[S(q)]}, \qquad (16.67)$$

where $D_s = D_0 H(\infty)$ is the short-time self-diffusion coefficient and $h(q) \equiv H(q)/H(\infty)$. For large particles, $[S(q)]/[h(q)] \to 1$. This occurs because the angular average in eqn (16.64) corresponds to a $q^3 F(q)$ weighted over the interval from 0 to $2k_0 R$ and strongly weights the high-q limit where both $S(q)$ and $h(q)$ approach 1. Using the Percus–Yevick form of $S(q)$ for hard spheres and the Beenakker–Mazur form for $H(q)/H(\infty)$, Xue et al.[22, 23] found that when the volume fraction ϕ is varied from 0 to 0.45, $[S(q)]/[h(q)]$ changes from 1 to 0.788 for 0.412 μm diameter spheres, from 1 to 0.921 for 0.913 μm diameter spheres. This indicates that, if the diameter of the suspending spheres is equal to or greater than ≈ 2 μm, the value of $[H(q)]$ is within 2 per cent of $H(\infty)$ for all ϕ. Thus, for $2R > 2$ μm, the measured values of D_{av} is essentially equal to the early-time self-diffusion coefficient, D_s. In the limit of large q where $D_{av} \approx D_s$, the off-diagonal terms in eqn (16.3) must average to zero, so that the single-scattering autocorrelation function is well approximated by eqn (16.5). Thus, for large particles, we can replace $D_{av}t$ in eqn (16.65), with $\langle r^2(t)\rangle$ and directly measure the mean-square displacement of particles over length scales much less than the wavelength of light.

16.2.6 *Mixtures*

In the preceding discussion we considered scattering only from monodisperse suspensions of colloidal particles. However, most colloids consist of a distribution of particle sizes. As a first step towards understanding DWS in polydisperse systems, we consider binary mixtures of two different particle sizes. Once this is done, the extension from binary mixtures to multicomponent systems is straightforward. In the single-scattering limit, scattering from particles of different sizes leads to multiple relaxation times and a non-exponential decay of $g_{(1)}(t)$. Analysis of this non-exponential decay can lead to at least partial information about the distribution of particle sizes. By contrast, in multiple scattering, particle polydispersity does not change the shape of the autocorrelation function and only average information about particle dynamics is obtained.

The basic effects of polydispersity are most readily understood by considering DWS in a binary mixture of non-interacting, uncorrelated spheres in

suspension.[14] The total volume fraction of the suspension is simply the sum of the volume fractions occupied by the individual species, $\phi = \phi_a + \phi_b$. We calculate the autocorrelation function by considering the phase shift for a light path of $N = n_a + n_b$ scattering events, with n_a and n_b scattering events from species a and b respectively:

$$\Delta\phi_p(z) = \sum_{i=1}^{N} \boldsymbol{q}_i \cdot \Delta\boldsymbol{r}_i(t) = \sum_{i=1}^{n_a} \boldsymbol{q}_{a_i} \cdot \Delta\boldsymbol{r}_{a_i}(t) + \sum_{i=1}^{n_b} \boldsymbol{q}_{b_i} \cdot \Delta\boldsymbol{r}_{b_i}(t). \qquad (16.68)$$

As in the case of a monodisperse suspension, we evaluate the average over phase factor by noting that $\Delta\phi_p(t)$ is a random Gaussian variable. Once again, the central limit theorem ensures Gaussian statistics for large N, even if the scattering properties of the two species are very different. Following the same reasoning as for the monodisperse case (see Section 16.2.3.1), we obtain an expression for the mean-square phase shift:

$$\langle\Delta\phi_p^2(t)\rangle = 2n_a\langle q_a^2\rangle D_a t + 2n_b\langle q_b^2\rangle D_b t, \qquad (16.69)$$

where we have assumed diffusive particle motion with $\langle r_i^2(t)\rangle = 6D_i t$ and $i = $ a, b. Because all particle positions are uncorrelated, we can evaluate the averages over scattering vectors separately and obtain

$$\langle q_i^2\rangle = 2k_0^2 \frac{l_i}{l_i^*}, \qquad (16.70)$$

where $l_i = 1/\rho_i\sigma_i$ and $l_i^* = l_i/(1 - \cos\theta)$ are the mean free paths and transport mean free paths corresponding to monodisperse suspensions with volume fractions ϕ_i of the individual species in the mixture. The average number of scattering events from each species in a given path of length N is proportional to the density and total scattering cross-section of each species. Thus the relative probabilities of scattering from species a and b is inversely proportional to their mean free paths,

$$\frac{n_a}{n_b} = \frac{\rho_a\sigma_a}{\rho_b\sigma_b} = \frac{l_b}{l_a}, \qquad (16.71)$$

or $n_a l_a = n_b l_b$. Substituting this result and eqn (16.70) into eqn (16.69) gives

$$\langle\Delta\phi_p^2(t)\rangle = 2k_0^2 n_a l_a (D_a/l_a^* + D_b/l_b^*)t. \qquad (16.72)$$

The total path length is given by $s = Nl'$, where l' is the mean free path of the mixture and includes scattering from both species. The inverse mean free path is simply the sum of the contributions from each species,

$$\frac{1}{l'} = \rho_a\sigma_a + \rho_b\sigma_b = \frac{1}{l_a} + \frac{1}{l_b}. \qquad (16.73)$$

Since $N = n_a + n_b = n_a(1 + l_a/l_b)$, it follows that

$$s = Nl' = n_a l_a. \qquad (16.74)$$

Thus eqn (16.72) becomes

$$\begin{aligned}
\langle\Delta\phi_p^2(t)\rangle &= 2k_0^2 s\left(\frac{D_a}{l_a^*} + \frac{D_b}{l_b^*}\right)t \\
&= 2k_0^2\left(D_a\frac{l_{eff}^*}{l_a^*} + D_b\frac{l_{eff}^*}{l_b^*}\right)\frac{s}{l_{eff}^*}t,
\end{aligned} \qquad (16.75)$$

where l_{eff}^* is the total transport mean free path and, for uncorrelated particles, is given by

$$\frac{1}{l_{eff}^*} = \frac{1}{l_a^*} + \frac{1}{l_b^*}. \qquad (16.76)$$

This result can easily be generalized to non-interacting multicomponent systems and is precisely the same result as we obtained for a non-interacting monodisperse system, but with an effective transport mean free path and an effective diffusion coefficient given by

$$\frac{1}{l_{eff}^*} = \sum_i \frac{1}{l_i^*} \qquad (16.77)$$

$$D_{eff} = \sum_i \frac{l_{eff}^*}{l_i^*} D_i. \qquad (16.78)$$

Therefore we obtain autocorrelation functions having precisely the same form as those for monodisperse systems, but with a time constant given by $\tau = (k_0^2 D_{eff})^{-1}$. The effective diffusion coefficient given in eqn (16.78) is simply the sum of the diffusion coefficients of the individual species weighted by their scattering power as measured by the inverse transport mean free path of each species.

The theory for non-interacting mixtures has been verified experimentally in dilute aqueous suspensions of 0.198 μm and 0.605 μm diameter spheres.[14] However, this theory cannot hold in concentrated or strongly interacting suspensions where correlations between particles are known to be important.[21] As for the case of monodisperse systems, interactions in polydisperse systems modify both the static and dynamic scattering properties of the suspension. The change in the static scattering is demonstrated by measurements, shown in Fig. 16.12, of the concentration-dependence of $1/l^*$ for several different binary suspensions. In this experiment, three binary mixtures of polystyrene spheres were used, each with the same ratio of particle diameters but with different
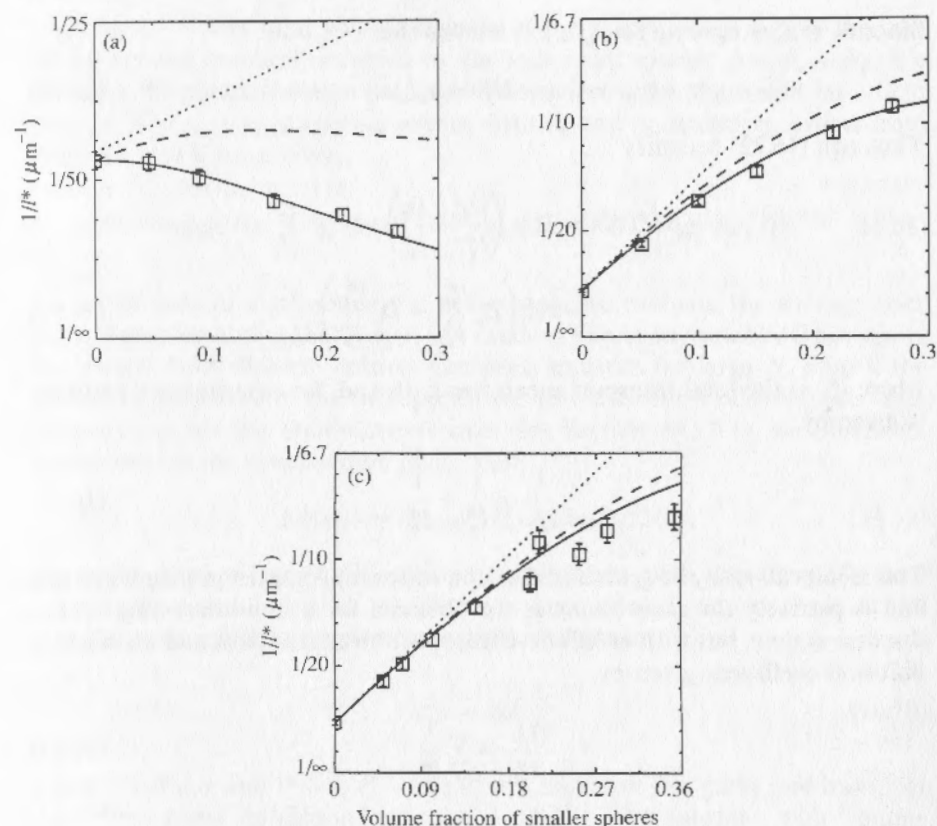
the scattering function appropriate for binary mixtures,

$$I(x)\rho = S_{LL}(x)F_L(x)\rho_L + S_{SS}(x)F_S(x)\rho_S + 2S_{LS}(x)\,\mathrm{Re}(f_L(x)\cdot f_S^*(x))\sqrt{\rho_L\rho_S},$$
(16.79)

where $F_\alpha(x) = |f_\alpha(x)|^2$ are the dimensionless, far field, single-scattering amplitudes for the small ($\alpha = S$) and large ($\alpha = L$) spheres. In this equation, the dimensionless scattering vector is chosen to be $x = qa_L$ and $\rho = \rho_L + \rho_S$. The partial structure factors are defined as sums over all particle positions r_i^α and r_j^β:

$$S_{\alpha\beta}(q) = \frac{1}{\sqrt{N_\alpha N_\beta}}\left\langle \sum_{ij}\exp(i\boldsymbol{q}\cdot(r_i^\alpha - r_j^\beta))\right\rangle,$$
(16.80)

The result for l^* in uncorrelated binary mixture given by eqn (16.76) is recovered from eqns (16.79) and (16.80) if the partial structure factors are set to $S_{\alpha\beta}(q) = \delta_{\alpha\beta}$.

For a system of hard spheres, the partial structure factors $S_{\alpha\beta}(q)$ have been calculated within the Percus–Yevick approximation,[24] while the far field scattering amplitudes can be calculated from Mie theory. Calculations of l^* using the Percus–Yevick structure factors and the Mie form factors are shown in Fig. 16.12 with the data for binary mixtures. The experiment and theory are in excellent agreement, The plots also show the results of calculations which ignore all interparticle structure ($S_{\alpha\beta}(q) = \delta_{\alpha\beta}$) and results which ignore only the correlations between different particle species ($S_{LS}(q) = 0$). It is particularly interesting to note that for the mixture with the smallest spheres, addition of the small colloidal particles actually causes $1/l^*$ to *decrease* with increasing ϕ_S. Physically, this is because the small spheres decrease the osmotic compressibility of the suspension and restrict the space available to the larger spheres, forcing the larger spheres into a somewhat more ordered liquid structure. At the same time, the small spheres are so much smaller than the wavelength of light, that they scatter very little light compared with the larger spheres in the mixture. The net effect of the increased order in the larger spheres and small additional scattering by the small spheres is to decrease the overall scattering of light and thus decrease $1/l^*$. These plots clearly illustrate the importance of using the full structure factor to model photon transport quantitatively.

The dynamical problem for interacting mixtures is not as well understood as the static problem. Part of the difficulty is because there are currently no calculations available for the full q-dependent collective diffusion coefficients for colloidal mixtures that interact strongly via the hydrodynamic interaction. Kaplan *et al.*[21] have proposed an effective q-averaged diffusion coefficient which includes hydrodynamic interactions but should be valid only in the large-particle ($R \gg \lambda$) limit. They obtain

$$D_{\mathrm{eff}} = \frac{D_{L0}[F_L(q)]\rho_L + D_{S0}[F_S(q)]\rho_S}{[I(q)]\rho},$$
(16.81)

FIG. 16.12. Measurements of the reciprocal photon transport mean free path $1/l^*$ show the effects of interparticle structure in binary colloidal mixtures of polystyrene spheres of (a) small, (b) medium, and (c) large overall size. Calculations using the full PY binary hard-sphere structure factors (——) agree with the data and differ most from a non-interacting theory (.....) and the theory without interspecies structure (– – –) when the particles are smaller than the wavelength of the probe.

absolute sizes. In each system, the volume fraction of the large spheres, ϕ_L, is held constant while the volume fraction of small spheres is varied from $\phi_S = 0$ to $\phi_S \approx 0.3$. For low ϕ_S, $1/l^*$ increases linearly with ϕ_S as expected from eqns (16.70) and (16.76) for uncorrelated systems. At higher ϕ_S, clear deviations from linear behaviour are observed.

To understand these measurements, we must account for the effect of correlations between particle positions on light transport. This can be done for binary mixtures by adapting the theory already developed for interacting monodisperse colloids. The starting point is eqn (16.58) for l^*. In a binary system, we can still use this equation but we must replace $I(x) = S(x)F(x)$ with

where [. . .] denotes the angular average prescribed by eqn (16.64) and D_{L0} and D_{S0} are the single-particle asymptotic short-time self-diffusion coefficients. These diffusion coefficients can be estimated from calculations by Batchelor.[25] Good agreement is achieved for the mixture with the largest particles. However, the theory fails to describe the data for the mixtures with the smaller particles, and this illustrates the need for a more comprehensive theory for the q-dependent diffusion coefficients which includes the hydrodynamic interactions between particles.

16.3 Applications

In this section we discuss some applications of diffusing-wave spectroscopy, both those with potential technological importance and those for the study of physical phenomena that cannot be addressed with conventional DLS. We begin with a discussion of the unique experimental considerations encountered with DWS that are not typical of other types of DLS experiment. Next we discuss the application of DWS to particle sizing of concentrated suspensions, and attempt to offer a critical assessment of the prospects and potential range of sizing applications that can be addressed. We then discuss a study of new phenomena for which we exploit the novel features of DWS and which could not have been investigated with conventional DLS scattering techniques. The first of these is the study of particle motion on very short length scales in concentrated colloidal suspensions. These measurements provide the first observations of the time evolution of hydrodynamic interactions between colloidal particles. They exploit the ability of DWS in the transmission geometry to measure motion of individual particles on very short length scales. The second example is the study of the dynamics of foams and the motion of the bubbles that occurs as the foam coarsens. This application exploits the very large volume of sample that is probed in a DWS experiment, as the bubble motion is spatially isolated, and in any given location, is temporally rare.

16.3.1 *Experimental considerations*

Diffusing-wave spectroscopy is dynamic light scattering from very highly scattering media. As such, it shares many of the experimental methods used for conventional DLS, particularly in the collection of the scattered light and the processing of the collected data. Just as in conventional DLS, the angular resolution of the detector must be limited to a single coherence area, or speckle spot. The intensity of this speckle is detected with a photomultiplier tube and standard photon counting electronics, and the resulting signal is analysed with a digital correlator. However, the fact that the light diffuses through the sample introduces new requirements that are unique to DWS. It is these new considerations that we discuss in this section.

The first major experimental difference between DWS and conventional DLS is in the basic geometries that can be effectively used, as has been discussed in Section 16.2. In conventional DLS, where the scattering vector is well defined, the angle of the detector can be adjusted to vary the scattering vector, q. In contrast, diffusing light leaves the sample with nearly uniform intensity in all directions, and thus the angle of the detector is not critical. Instead, the only important element of the geometry is whether the scattering is backscattering or transmission. Each geometry has its own features, and the choice between them will depend on the goals of a particular experiment.

One experimental requirement that is much more stringent for DWS than for normal DLS is the power of the laser source. It might seem that the very highly scattering samples studied with DWS will produce an abundance of scattered light intensity. While this is true, the fact that the light diffuses within the sample means that the light spreads throughout a large volume of the sample and leaves in all directions. Since only a small portion of the outgoing light is collected, considerably more laser power is required. The transmission geometry places the more stringent requirements on the incident power. A typical sample geometry for a transmission experiment is a slab of thickness L and of lateral extent much greater than L. The incident beam is typically focused to a spot much smaller than L on one side of the sample. Diffusive propagation of the light through the sample causes it to spread to illuminate an area of radius $\approx L$ on the other side of the sample. This will have a very deleterious effect on the useful signal for a dynamic light scattering measurement. Since the light leaves the sample uniformly in all directions, the intensity at a detector of area A a distance R from the sample will be roughly (A/R^2). For a dynamic light scattering experiment, the detector area should be roughly a single coherence area, and since the size of the scattering source on the sample is $\approx L$, the coherence criterion requires that $A = (R\lambda/L)^2$. In addition, the transmission of light diffusing through a slab decreases as l^*/L. Thus the useful intensity for a dynamic light scattering experiment, which is the intensity per speckle spot, falls as $l^*\lambda^2/L^3$. Since $l^* \ll L$ and $\lambda \ll l^*$, this puts large demands on the input laser power. These demands are actually more severe for more weakly scattering samples, where l^* is larger, as these samples must be thicker. Thus HeNe lasers often do not provide sufficient power for DWS experiments, and more powerful Ar^+ or Kr^+ lasers are usually required.

The sample thickness requirements for DWS also ensures that virtually no unscattered light is transmitted through the sample. For the diffusion approximation to be valid, the sample thickness must be at least several times greater than l^*. In fact, the expressions for the DWS correlation functions are most appropriate for $L/l^* \geqslant 5$, so that the effects of internal reflections do not modify the boundary conditions and hence increase the apparent thickness. In this case, the attenuation of unscattered light transmitted though the sample will fall as $\exp(-L/l)$. Since l^* is typically several times greater than l, virtually no unscattered light will be transmitted through the sample. Thus samples that

can be studied with DWS cannot typically by studied with other DLS techniques that reduce the effects of multiple scattering by cross-correlation techniques of the signals detected at two angles or with two different colours. Both of these cross-correlation techniques are designed to eliminate the effects of multiple scattering by measuring the cross-correlation of two different speckle spots that reflect the same motion of the particles. Only singly-scattered light contributes to the cross-correlated signal from the two speckles, so these techniques effectively eliminate the effects of multiple scattering. However, both techniques rely on there being sufficient unscattered light reaching each of the detectors. This will not occur for samples used in most DWS experiments.

An additional constraint on the incident power is imposed by the fact that multiply-scattered light is depolarized. Thus if the incident light is linearly polarized, multiply-scattered light will have essentially equal intensities both parallel and perpendicular to the incident beam. Each polarization channel is independent, reducing the intercept, and hence the signal-to-noise ratio, of the correlation function by a factor of two if no polarization analyser is used in front of the detector. Although the use of a polarization analyser will restore the intercept, the total scattered intensity will be reduced. This places further demands on the incident power required to obtain a good signal. In fact, if the light is not completely depolarized, the use of an analyser to measure only depolarized scattered light will ensure that only multiply-scattered light is detected. This can be particularly useful in the backscattering geometry, where small particles, which scatter light more isotropically, yield a significant amount of singly-scattered light, which is not depolarized and cannot be properly treated within the diffusion approximation.

A final constraint on the incident power is imposed by absorption in the sample. As discussed above, the consequences of absorption are much more severe for multiply-scattered light than for singly-scattered light, since the path lengths are so much longer. Even weak absorption in a sample will result in a modification of the shape of the autocorrelation function, and this must be included in the analysis. Ideally it is preferable to measure the absorption length independently, in the absence of large scattering, and include this in the analysis. However, this is often not possible, and an absorption length must be determined in the data analysis from the shape of the autocorrelation function.

The description of the transport of light using the diffusion approximation also imposes unique requirements on the sample geometry. To use effectively the functional forms derived in Section 16.2, the sample must be large enough, and have a suitable geometry, to ensure that the light paths are not cut off by the shape or the finite size of the sample. The constraints placed on the sample geometry can be easily understood on physical grounds. In the transmission geometry, the characteristic path length is L^2/l^*. If the incident beam is focused on one face of the sample, the diffusion of the light causes it to expand to an area of roughly L in radius at the other side of the sample. Thus the lateral extent of the sample must be several times its thickness to ensure that light

paths are not cut off. This same requirement also determines the minimum size of the incident beam when it is expanded to illuminate the full face of the sample.

The sample thickness is one parameter that is experimentally controllable, as it can be used to adjust the amount of motion per particle required to cause the decay. As such, thicker samples are sometimes desirable, putting larger demands on laser power. The incident laser intensity is most efficiently used when the incident beam is focused on the sample, but this can cause potential problems with power density at the sample face. Thus it may be desirable to defocus the incident beam slightly. The requirements of a point focus assumed in the derivation of the correlation function imply only that the incident laser be focused to a spot that is substantially smaller than the thickness of the cell. Thus as L increases, the constraints of a very tight focus are relaxed. The results for the autocorrelation function for a larger-sized beam can be calculated using eqn (16.42).

Similar requirements also pertain to the backscattering geometry. In this case however, paths of all lengths contribute, depending on how early in time the correlation function is to be measured. Earlier times have contributions from longer paths and thus require a sample of larger extent. The extent can be easily estimated by considering the simple case of non-interacting Brownian spheres, where τ_0 is known. For this system, a path of length s decays in a time $\tau = \tau_0 l^*/s$. However, since $s \approx L_s^2/l^*$, where L_s is the spatial extent of a diffusive path of length s, the sample thickness must be at least $L_s = l^*\sqrt{\tau_0/\tau}$. Similarly, since these paths arise from laser light incident a distance L_s from the spot where the light is detected, the sample must also be larger than L_s and the incident beam must illuminate a spot that is larger than L_s.

The large path lengths characteristic of DWS also place much more severe requirements on the coherence of the laser. These requirements need not be considered at all in conventional DLS. The physics of these coherence requirements is again straightforward: DWS measures the loss in phase coherence of a path due to the motion of the scatterers. If the laser coherence length is shorter than the path length, an additional dephasing mechanism is introduced. This essentially cuts off paths longer than the coherence length, and can change both the intercept of the intensity correlation function and its shape. Lasers typically used for DLS, such as Ar^+ and Kr^+ lasers, operate in many longitudinal modes, giving them a coherence length of only a few centimetres. However, the coherence length of the laser is increased to several metres by forcing it to operate in a single longitudinal mode, using an intercavity etalon. This ensures that the coherence length is much larger than the characteristic path length, so that all the dephasing of the light results solely from the particle motion. This is often essential for DWS, quite unlike conventional DLS, to avoid the deleterious effects of such a short coherence length, and to study thicker samples.

The correlation functions measured with DWS decay much faster than those

measured with conventional DLS, placing more demands on the time resolution of the correlator. This has actually inspired the development of new real-time correlators that are faster than those designed for conventional DLS. Real-time digital correlators with minimum sample times as short as 12.5 ns are now commercially available, and meaningful data can be obtained using these correlators and DWS in the transmission geometry. However, the use of these high-speed correlators introduces additional requirements on the experiment. The use of an intercavity etalon in the laser is essential, since the beat frequency between adjacent longitudinal modes can be resolved by the high speed of the correlator. In addition, problems of dead time in the photon counting equipment become much more severe, as do problems with correlated after pulsing of the photomultiplier used as the detector. Both effects can be greatly reduced by placing a beam splitter after the final pinhole and using two separate photomultiplier tubes in a cross-correlation mode. Finally, if the sample is sufficiently thick, the decay becomes so rapid that temporal correlation techniques are no longer practical. Then the autocorrelation function must be measured in the frequency domain using interferometric techniques with a Fabry–Perot or Michelson interferometer. In fact, Yodh *et al.*[26] have been able to measure the decay of the electric field autocorrelation function of thick, multiple-scattering samples using a Michelson interferometer. With this technique they have been able to resolve motion on a 0.01 nm length scale. Thus the very earliest stages of Brownian motion can be probed.

16.3.2 *Particle sizing*

The measurement of the size and polydispersity of colloidal particles is one of the most important applications of conventional DLS, and has stimulated much of its development. However, many suspensions of technological importance are quite concentrated, exhibiting high multiple scattering, and thereby severely limiting the applicability of conventional DLS. For this reason, particle sizing of concentrated suspensions holds the promise of ultimately becoming one of the most important applications of DWS. Unfortunately, however, this application has to date found somewhat limited use, and requires considerably more development before it can match the widespread utility of conventional DLS. Here we discuss possible schemes for employing DWS for particle sizing, and indicate the areas where further theoretical and experimental development would be most beneficial. We also review some successful applications of DWS to particle sizing that have already been reported.

Perhaps the conceptually simplest technique for measuring particle size uses the backscattering geometry. This geometry has the advantage that only a single optical access is required. This could for example be a window in a processing container. Furthermore, no additional knowledge of the scattering properties of the suspension is required, since the autocorrelation function does not depend on the value of l^*. Unfortunately, despite its inherent simplicity, backscattering

is also the least well understood geometry, where the diffusion approximation is most suspect. As discussed above, this is a result of the relatively large contribution of short paths, of length less than l^*, to which the diffusion approximation does not apply.

Despite the limitations, useful particle size information can still be obtained using DWS in backscattering. This is predicated on the form of the autocorrelation for backscattering, which is typically quite well approximated by eqn (16.46), $g_{(2)}(t) \approx \exp(-\gamma\sqrt{6t/\tau_0})$. Thus a determination of $dg_{(2)}(t)/d\sqrt{t}$ provides a measure of $\gamma/\sqrt{\tau_0}$. To a reasonable approximation, accurate to about 20 per cent, γ can be chosen to be 2.1.[12] This then provides a measure of τ_0, and hence of the particle size. This measurement can be refined by exploiting the fact that the value of γ reflects the contribution of short paths, and hence varies with the polarization of the scattered light detected, compared with the incident light. Thus, for example, for parallel polarization there is an additional contribution of short paths that decay more slowly, thus decreasing the value of γ for the parallel polarization channel of the scattered light as compared with the perpendicular polarization channel of the scattered light. This effect is more pronounced for smaller particles, which tend to scatter light more anisotropically, and hence have a relatively larger amount of scattered intensity in the parallel polarization channel. In fact, the ratio of the values of γ measured in each of the linear polarization channels can be used to refine the measurement of τ_0. This can be seen in the results shown in Fig. 16.13, which is a plot of the value of γ obtained using suspensions at $\phi \approx 0.01$ with different sphere sizes. As can be seen, as the particle size increases, and hence the scattered intensity
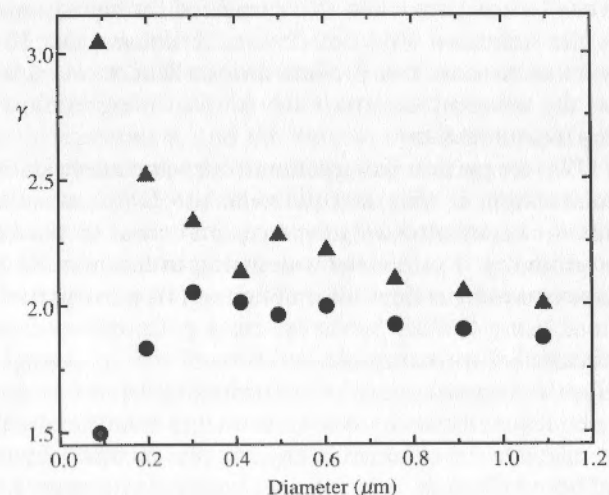

FIG. 16.13. Values of γ for both the parallel (●) and the perpendicular (▲) polarization channels, as a function of particle size. Measurements of both polarization channels can reveal information about particle size.

in each of the polarization channels becomes more nearly identical, the values of γ for both channels approach 2.1. In contrast, as the particle size decreases, so that the contribution of singly-scattered paths increases, the values of γ diverge, with $\gamma_\parallel$ decreasing compared with $\gamma_\perp$ since there is a large contribution from single-scattered paths that decay more slowly. If a plot of the sort shown in Fig. 16.13 is available for the samples of interest, then measurement of the autocorrelation function for each polarization can be used to refine the size determination of the particles. We note however that studies of the dependence of γ on particle size have been limited. While the behaviour shown in Fig. 16.13 is certainly observed for monodisperse, spherical particles at concentrations of a few per cent, the behaviour of suspensions with higher concentrations, more polydispersity, or more irregular-shaped particles has not been extensively investigated. This must be done to ensure the more general applicability of DWS for measuring particle size in concentrated suspensions. More importantly, the theory for DWS in backscattering must be refined, and a more fundamental understanding of the parameter γ must be developed to exploit fully the potential of DWS for particle size measurements.

Unlike backscattering, transmission measurements do not suffer from the same uncertainties in the theoretical interpretation of the data. However, transmission measurements are somewhat more complex, since they require two optical accesses to the sample. Moreover, interpretation of the data also requires independent knowledge of the value of l^*, since the autocorrelation function always depends on the product of l^* and τ_0. This can in principle be obtained by measuring the total light transmission through the sample in a static measurement. Provided that an identical optical arrangement is used, the transmission can be compared with that measured through a sample of known l^*, and thus the unknown value of l^* can be determined. If this is done, transmission measurements can provide an excellent measure of the particle size, without the inherent uncertainties in the interpretation that plague backscattering measurements.

The use of DWS for particle sizing suffers from some unavoidable drawbacks. Additional information is always required to use DWS, as either γ must be determined for the backscattering geometry, or l^* must be determined for the transmission geometry. Furthermore, unlike conventional DLS, with poly-disperse samples no independent information about particle size distributions can be obtained using DWS. Physically, every path scatters from all sizes of the particles in a polydisperse sample, and thus reflects an average over particle size, even before the contributions of individual paths are averaged. Thus no information about polydispersity can be extracted from the data. However, it is possible to calculate the expected behaviour of a mixture of particle sizes, as was discussed above. Thus in principle it is possible to compare the data with the predicted behaviour assuming some model distribution, and thereby check the validity of the model. Finally, an additional problem can arise in the interpretation of the results because of particle interactions. These can be very

large at the high volume fractions of the suspensions which can be studied with DWS. Both potential interactions, as characterized by $S(q)$, and hydrodynamic interactions, as characterized by $H(q)$, will modify the effective diffusion coefficient measured in a DWS experiment. As discussed above in Section 16.2.5, DWS measures a weighted average of these functions over the full range of q accessible with the wavelength used. The effects of $S(q)$ tend to be compensated by those of $H(q)$, and the net effects are reduced. If these functions are known, it is possible to interpret the data correctly, accounting properly for the effects of the interactions. This is certainly the case for particles interacting by a hard-sphere potential, where both $S(q)$ and $H(q)$ are known. Actually, even for other interaction potentials, the effects of the interactions may often not be substantially different from the hard-sphere case. At high volume fractions, packing constraints dominate the potential interactions, and $S(q)$ determined for the hard-sphere interaction is likely to be a reasonable approximation for many other types of interactions. At low concentrations, the effects of $H(q)$ are greatly diminished, while the effects of $S(q)$ will primarily differ at relatively small values of q, which make a less important contribution to the average because of the q^3 weighting. This will be particularly true for larger particles. Thus the effects of interactions will typically be included in a reasonably straightforward fashion.

There have not been extensive reports to date of attempts to use DWS for particle sizing. Nevertheless, DWS has been successfully applied to study aggregation processes in milk during the formation of cheese. Horne[27] has used an elegant experimental arrangement employing a bifurcated optical fibre bundle. Light is injected through one half of the bundle, and is emitted from fibres randomly situated at the face of the other end of the bundle, which is immersed in the milk sample. The scattered light is detected through only a single fibre in the second half of the bundle. This fibre is chosen to be situated near the centre of the face. This provides a simple scheme for performing DWS backscattering measurements, and the data so obtained are well described by the formalism discussed above, enabling the average particle size to be measured. With this scheme, Horne[27] was able to study both the early aggregation process in the initial stages of cheese-making, as well as the later formation of a gel network as the cheese aged. This is a good example of the potential of DWS to provide useful particle size measurements in highly scattering samples without the requirement for dilution.

Despite its drawbacks, DWS remains the only method for measuring particle sizes in concentrated suspensions that exhibit high multiple scattering. As such, it should find considerable use. At its present level of development, DWS is probably most suitable as an analytical technique that can be used for monitoring the progress of some process that is reasonably well understood, rather than as an independent technique that can by itself give detailed and exact information about particle size. Instead, DWS is more suitable for following changes in the average particle size, with other more precise techniques

being used to initially determine the particle size and its distribution. For example, dilution and then conventional DLS could be used initially to measure the particle size at different stages of processing, and then the DWS results could be correlated with the more conventional results. Then DWS could be used as an *in situ* monitor of the process. More development of both the experimental technique and the theory of DWS is clearly highly desirable. This would help to identify the optimum geometry and techniques for different applications. With this further development, DWS might achieve its promise of providing a light scattering method for measuring particle size in concentrated suspensions.

16.3.3 *Particle motion on short length scales*

Diffusing-wave spectroscopy provides a unique method for probing physical phenomena that cannot otherwise be studied. The motion of a particle one micrometre in diameter can be resolved on length scales as short as several ångströms. Physically this can be achieved because DWS measures the time taken for the total length of a diffusive light path to change by one wavelength. This path can consist of a very large number of scattering events. Thus the motion of each scatterer need be only a very small fraction of a wavelength. In addition, the time-scales for these very small motions will be correspondingly shorter. The physics of motion at these very short length and time scales can be significantly different from that of motions typically probed by conventional DLS, which are on length scales comparable with one wavelength and on time-scales that are correspondingly longer.

To illustrate the power and utility of DWS in studying new physical phenomena at these short length and time scales, we concentrate on one example. At sufficiently short time and length scales, the motion of Brownian particles is no longer simply diffusive in nature. Instead, it directly reflects the consequences of hydrodynamic interactions, both between the particle and the surrounding fluid, and between the particle and other neighbouring particles, mediated by the viscous fluid. Here we discuss the use of DWS to measure motion of colloidal particles at very short length and time scales and to study hydrodynamic interactions in concentrated suspensions.

Hydrodynamic interactions play a critical role in determining the dynamic properties of fluid suspensions of all sorts. However, hydrodynamic interactions are extremely difficult to treat theoretically because they are intrinsically many-body in nature. Furthermore, although their consequences have been widely studied experimentally, the actual time evolution of hydrodynamic interactions has not been investigated. Hydrodynamic interactions are not a static or potential form of interaction, and thus do not affect the average structure of a suspension, as characterized for example by the structure factor, $S(q)$. Instead, hydrodynamic interactions result from the motion of the particles in the fluid and the viscous coupling of this motion to the fluid and to other

particles. The time-scale of this coupling is set by the kinematic viscosity of the suspension, η/ρ, where η is the shear viscosity and ρ is the density of the fluid. The kinematic viscosity is the diffusion coefficient that determines the rate of diffusion of momentum in a viscous fluid. It determines the time-scale over which the fluid flow can change. Typically the time-scale for the propagation of hydrodynamic interactions is so rapid that they are viewed as instantaneous. However, hydrodynamic interactions are in fact retarded interactions, as there is a finite time for their propagation. The use of DWS in the transmission geometry makes it possible to probe the motion of colloidal particles on sufficiently short time and length scales to monitor experimentally the time evolution of hydrodynamic interactions. Furthermore, since concentrated suspensions are essential for the use of DWS, hydrodynamic interactions can be studied as the particle concentration is increased.

To consider the transient nature of hydrodynamic interactions, we begin with the description of a single Brownian particle in a viscous fluid, as some of the assumptions typically made in conventional DLS are no longer adequate when considering the time and length scales probed with DWS. Thus we describe the particle's instantaneous position by $r(t)$ and its instantaneous velocity by $v(t)$, so that

$$r = \int_0^t v(t')\,dt' \qquad (16.82)$$

The particle motion is described by the Langevin equation,

$$m\dot{v} = -\zeta_0 v + f(t), \qquad (16.83)$$

where m is the mass of the particle, ζ_0 is the friction coefficient, and $f(t)$ is a random thermal force exerted on the particle by the collisions of the fluid molecules. For a spherical particle of radius a, the zero-frequency friction coefficient is given by $\zeta_0 = 6\pi\eta a$. The use of the Langevin equation implicitly assumes that the time-scale of the collisions of the individual molecules with the particle is much more rapid than the motion of the particle, so the effect of these collisions can be replaced by a random fluctuating force. The time-scale of the individual collisions of the fluid molecules is of the order of 10^{-13} s, while the time-scale of the transient hydrodynamic interactions is greater than 10^{-8} s. Thus the Langevin equation is a suitable description for the time-scales of concern here. Furthermore, the random force can be assumed to be a stationary Gaussian random process.

The Langevin equation is normally solved by assuming that the friction coefficient is a constant. Then the particle's velocity is

$$v(t) = v(0)\,e^{-t/\tau_B} + \int_0^t d\tau\,e^{-(t-\tau)/\tau_B} f(t), \qquad (16.84)$$

where the Brownian time, $\tau_B = m/\zeta_0$, is the viscous damping time, in which the

particle's velocity is damped out owing to the viscosity of the fluid. Because of the random nature of the forces, it is more meaningful to consider the particle's velocity autocorrelation function,

$$R(t) = \langle \mathbf{v}(0) \cdot \mathbf{v}(t) \rangle. \tag{16.85}$$

Using eqn (16.84), we have

$$R(t) = R(0) \, e^{-t/\tau_B} + \frac{1}{3} \int_0^t d\tau \, e^{-(t-\tau)/\tau_B} \langle \mathbf{v}(0) \cdot \mathbf{f}(t) \rangle. \tag{16.86}$$

Because of causality, the particle's velocity at $t = 0$ cannot depend on the random force some time later, so that $\langle \mathbf{v}(0) \cdot \mathbf{f}(t) \rangle = 0$, and the second term does not contribute. In addition, from equipartition, the initial value of the velocity autocorrelation function is given by $R(0) = k_B T/m$, giving

$$R(t) = \frac{k_B T}{m} \, e^{-t/\tau_B}. \tag{16.87}$$

The mean-square displacement of the particle, $\langle \Delta r^2(t) \rangle$, is given in terms of the velocity autocorrelation function,

$$\langle \Delta r^2(t) \rangle = 6 \int_0^t dt' (t - t') R(t'). \tag{16.88}$$

At sufficiently long times, the velocity autocorrelation function must decay to zero, and using eqn (16.87), we can define the self-diffusion coefficient, D_0, by

$$\langle \Delta r^2(t) \rangle = 6 D_0 t. \tag{16.89}$$

This is the asymptotic value of the diffusion coefficient, reached after the velocity autocorrelation function has decayed but before the particle has moved far enough to interact with the potential of its neighbours. Thus by D_0 we refer to what is often called the short-time self-diffusion coefficient. For dilute suspensions, D_0 is given by the Stokes–Einstein formula, $D_0 = k_B T/\zeta_0$. However, since we wish to consider the particle motion at time-scales comparable with the decay of $R(t)$, the diffusion coefficient is no longer a constant, and we define the time-dependent diffusion coefficient,

$$D(t) = \int_0^t dt' R(t'). \tag{16.90}$$

Using eqn (16.87), we have

$$D(t) = D_0(1 - e^{-t/\tau_B}). \tag{16.91}$$

The mean-square displacement can also be expressed in terms of the time-dependent diffusion coefficient,

$$\langle \Delta r^2(t) \rangle = 6 D_0 [t - \tau_B(1 - e^{-t/\tau_B})]. \tag{16.92}$$

A basic assumption made in obtaining all of these results is that the particle velocity is viscously damped by the fluid in the Brownian decay time, τ_B. This leads to an exponential decay of the velocity autocorrelation function, and a corresponding exponential rise of the time-dependent diffusion coefficient to its asymptotic value. In addition, $\langle \Delta r^2(t) \rangle$ exponentially approaches the linear dependence on time expected for diffusive motion of the colloidal particle. This approach is adequate for the description of particle motion studies using conventional DLS, since the motion of the colloidal particles during the decay of the velocity autocorrelation function cannot be observed. Consider, for example, a 1 μm diameter polystyrene sphere in water at room temperature. Its Brownian decay time is $\tau_B = 33$ ns, while the initial value of its velocity autocorrelation function is $R(0) = 13.7$ cm^2 s^{-2}. Thus in a Brownian decay time, the particle would move only ≈ 1.2 nm, and motion of this scale would not be detected by conventional DLS. In contrast, with DWS we can measure motion on length scales of this magnitude. Thus the approximation discussed above, which is typically made, must be reconsidered.

The problem with this approximation lies in the use of a constant value for the friction coefficient. This ignores the effects of the particle motion on the flow of the surrounding fluid. These can be described by including inertial and memory terms in the Langevin equation:

$$m\dot{v}(t) = \zeta_0 v(t) - \tfrac{2}{3}\pi\rho a^3 \dot{v}(t) - 6a^2(\pi\eta\rho)^{1/2} \int_{-\infty}^t \frac{\dot{v}(t')}{(t-t')^{1/2}} \, dt' + F(t). \tag{16.93}$$

This equation can be solved by Laplace transform techniques, leading to a more complex expression for the velocity autocorrelation function.[28] We express the result in terms of the dimensionless time, $\tau = t/\tau_v^0$, where $\tau_v^0 = a^2\rho/\eta_0$ and η_0 and ρ are the viscosity and density of the fluid:

$$R(\tau) = \frac{k_B T}{m} \frac{2\Sigma}{3\sqrt{5 - 8\Sigma}} \left[\alpha_+ \, e^{\alpha_+^2 \tau} \text{erfc}(\alpha_+\sqrt{\tau}) - \alpha_- \, e^{\alpha_-^2 \tau} \text{erfc}(\alpha_-\sqrt{\tau}) \right]. \tag{16.94}$$

The ratio of particle to fluid densities is given by $\Sigma = \rho'/\rho$, erfc(x) is the complex complement of the error function, and

$$\alpha_\pm = \frac{3}{2} \frac{3 \pm \sqrt{5 - 8\Sigma}}{1 + 2\Sigma}. \tag{16.95}$$

The corresponding expressions for the time-dependent diffusion coefficient and

the mean-square displacement are

$$D(\tau) = D_0 \left\{ 1 + \frac{3}{\sqrt{5 - 8\Sigma}} \left[\frac{e^{\alpha_+^2 \tau}}{\alpha_+} \operatorname{erfc}(\alpha_+ \sqrt{\tau}) - \frac{e^{\alpha_-^2 \tau}}{\alpha_-} \operatorname{erfc}(\alpha_- \sqrt{\tau}) \right] \right\} \quad (16.96)$$

and

$$\langle \Delta r^2(\tau) \rangle = 6 D_0 \tau_v \left\{ \tau - 2\sqrt{\frac{\tau}{\pi}} + \frac{2}{9}(4 - \Sigma) + \frac{3}{\sqrt{5 - 8\Sigma}} \right.$$
$$\left. \times \left[\frac{1}{\alpha_+^3} e^{\alpha_+^2 \tau} \operatorname{erfc}(\alpha_+ \sqrt{\tau}) - \frac{1}{\alpha_-^3} e^{\alpha_-^2 \tau} \operatorname{erfc}(\alpha_- \sqrt{\tau}) \right] \right\}. \quad (16.97)$$

When the full time-dependent viscosity is used, the velocity autocorrelation function no longer decays exponentially, but instead decays algebraically. At long times, its limiting behaviour is

$$\lim_{t \to \infty} R(t) = \frac{D_0}{2\tau_v^0 \sqrt{\tau}} \left(\frac{t}{\tau_v^0} \right)^{-3/2}. \quad (16.98)$$

This is the 'long-time tail' in the velocity autocorrelation function, which has a $t^{-3/2}$ power-law decay. The corresponding behaviour for the time-dependent diffusion coefficient results in a $t^{-1/2}$ approach to its asymptotic value.

These transient hydrodynamic effects can be directly observed by using DWS. To facilitate their observation, the viscous time-scale should be made as large as possible by using larger-diameter spheres. This also considerably simplifies the interpretation of the data, since it ensures that the self-diffusion coefficient is measured, as discussed in Section 16.2.5.

To investigate these effects, we use 1.53 μm diameter polystyrene latex spheres in water. The counterion concentration is sufficiently high to ensure a short Debye–Hückel screening length, resulting in a hard-sphere interaction between the particles. A volume fraction of $\phi = 0.021$ ensures sufficient multiple scattering to enable the DWS formalism to be used, but is low enough for the interactions between the particles to be minimized, with both $S(q)$ and $H(q)$ approximately unity over the full range of q accessed by the scattering. To measure motion on the very short length scales required, DWS in the transmission geometry is used. Furthermore, to obtain adequate signal-to-noise ratio at the very short time-scales required, the data are collected for approximately 12 hours. However, the sample is rotated every 10 min to ensure that the concentration does not change owing to gravitational sedimentation over the course of data collection. A high-speed, real-time digital correlation is used to measure the temporal autocorrelation function of the scattered light to delay times as short as 12.5 ns. The measurement of autocorrelation functions at these

short delay times requires careful attention to the experimental arrangement. To reduce the effects of spurious correlations due to afterpulsing in the photomultipliers, and also to reduce the effects of dead time in the electronics, a beamsplitter is placed after the final pinhole of the detection optics to direct the signal to two photomultipliers, whose output is cross-correlated. In addition, an intercavity etalon must be used to force the laser to oscillate in a single longitudinal mode to avoid detection of mode beating in the correlation function. With these precautions, good-quality correlation functions can be obtained at these short time-scales using DWS.

The data are analysed using the DWS formalism to determine $\langle \Delta r^2(t) \rangle$ directly. A zero-crossing routine is used to invert eqn (16.41) and obtain $k_0^2 \langle \Delta r^2(t) \rangle (L/l^*)^2$. Then, using the value of l^* calculated from Mie theory, the mean-square displacement of the particles is determined. These results are shown in a double logarithmic plot in Fig. 16.14. Motion on length scales as short as a few ångströms can be clearly resolved, demonstrating the sensitivity of DWS. To illustrate more clearly the effects of the long-time tail of the velocity autocorrelation function, we numerically differentiate the data to obtain the time-dependent diffusion coefficient. The differentiation is done by fitting the data to a third-order polynomial. The range of the fitted data is always chosen to be about one decade in time, improving the signal-to-noise ratio of the derivative without causing significant loss in the time resolution of the results. The time-dependent diffusion coefficient is shown in Fig. 16.15. The solid line through the data is the result predicted theoretically using the time-dependent
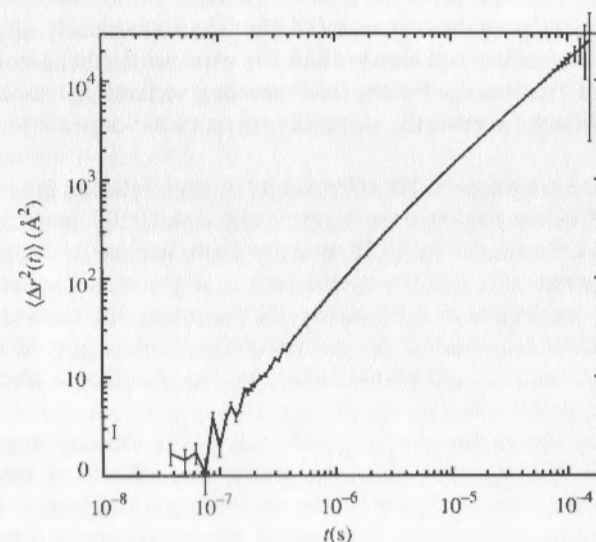

FIG. 16.14. Logarithmic plot of the time evolution of the mean-square displacement measured using DWS for 1.53 μm diameter particles at $\phi = 0.021$.
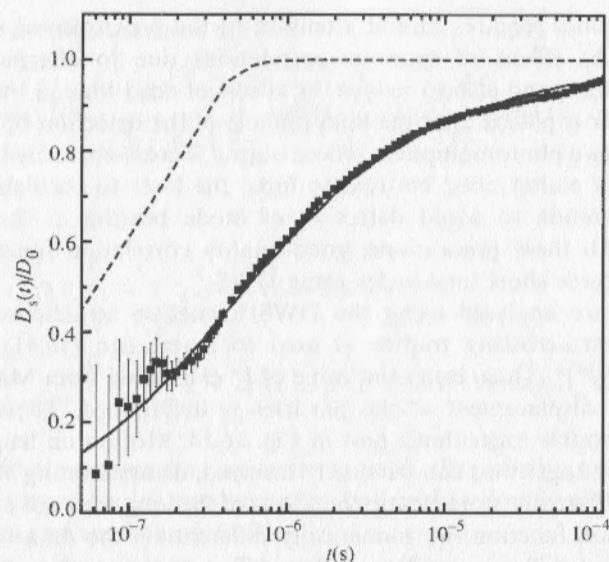
FIG. 16.15. Plot of the time evolution of the self-diffusion coefficient for 1.53 μm particles for $\phi = 0.021$. The solid line is the theoretical prediction, eqn (16.96), using the time-dependent friction factor. The dashed line is the theoretical prediction, eqn (16.91), using the time-independent friction factor.

diffusion coefficient predicted by eqn (16.91). The data clearly approach their asymptotic value much more slowly than the exponential behaviour predicted with a constant friction coefficient, and are in excellent agreement with the behaviour predicted theoretically using the correct time-dependent form for the friction.

To observe the long-time tail in the velocity autocorrelation function directly, the second derivative can also be numerically calculated to determine $R(t)$. These results are shown in Fig. 16.16, and are again in excellent agreement with the theoretical prediction, shown by the solid line through the data. The data clearly exhibit the predicted $t^{-3/2}$ decay, as shown by the dashed line. These results are a clear illustration of the power-law behaviour of the velocity autocorrelation function, and would simply not be obtainable without the use of DWS.

In addition to measuring the long-time tail in the velocity autocorrelation function, DWS can also be used to study the effects of hydrodynamic interactions on the time evolution of the self-diffusion coefficient. This can be done by increasing the volume fraction of the suspensions. Physically, the increasing volume fraction will lead to hydrodynamic interactions between the neighbouring particles, since the fluid flow will be disrupted by the presence of
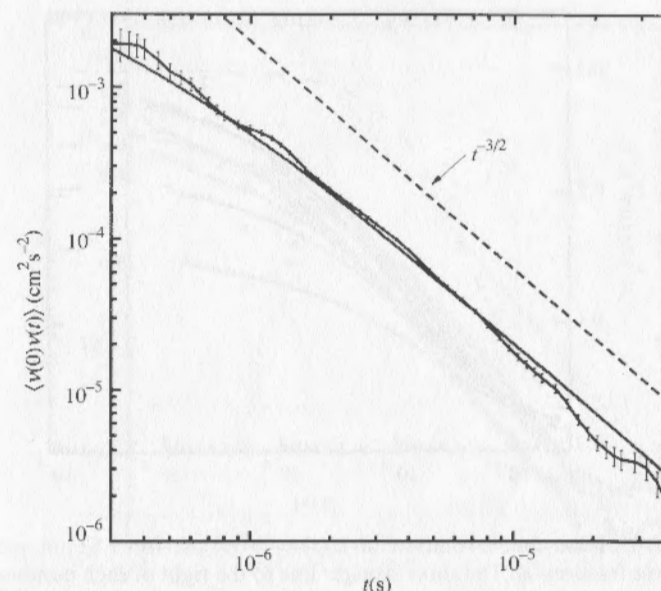
FIG. 16.16. Logarithmic plot of the velocity autocorrelation function for 1.53 μm diameter particles for $\phi = 0.021$. The solid line is the theoretical prediction, eqn (16.94). The $t^{-3/2}$ 'long-time tail' is apparent.

the nearby particles as the vorticity diffuses out from the tracer. Hydrodynamic interactions between neighbouring particles are traditionally viewed as instantaneous, since it has previously not been possible to measure experimentally their time-scale. However, hydrodynamic interactions are in fact retarded, taking a finite amount of time to propagate between particles. This can be directly observed with DWS.

To investigate these effects, we again use 1.53 μm diameter polystyrene latex spheres, and make DWS measurements in transmission for different volume fractions. The volume fractions are measured by drying and weighing a small portion of the suspension. Data are again collected with the very high-speed correlator, and the autocorrelation functions are averaged for about 12 hours to obtain sufficiently good statistics at the shortest delay times. In addition, the measured baseline due to laser fluctuations is subtracted from the data, enabling us to measure the decay in the intensity autocorrelation function, $g_{(2)}(t)$, over almost four orders of magnitude. The field autocorrelation functions are determined from the data, and are inverted using eqn (16.41). We use the value of l^* calculated using Mie theory. To reduce the statistical uncertainty inherent in numerically differentiating the data, we use an alternative definition for the time-dependent self-diffusion coefficient, $D_s(\tau) \equiv \langle \Delta r^2(\tau) \rangle / 6\tau$. The results for samples with several different values of ϕ are shown in Fig. 16.17. The highest
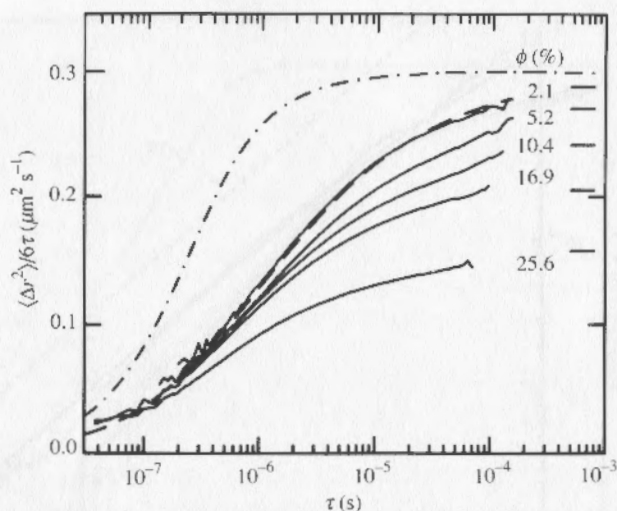
FIG. 16.17. Plot of the time evolution of $D_s(t) = \langle r^2(t) \rangle/6t$ for 1.53 μm particles for different volume fractions ϕ. The short straight line to the right of each number indicates the asymptotic short-time self-diffusion coefficient predicted by Batchelor[25] for each volume fraction. The dashed line through the 2.1 per cent data is the theoretical prediction for $\langle r^2(t) \rangle/6t$ of Hinch.[28] The dash-dot line is the theoretical prediction for $\langle r^2(t) \rangle/6t$ using eqn (16.92) with a time-independent friction factor.

curve repeats the data for $\phi = 0.021$ shown previously. It is again compared with the theoretical prediction, shown by the dashed line; the data and the theory are nearly indistinguishable. The data for the higher volume fractions are markedly different. As the volume fraction increases, the asymptotic value that the data approach decreases markedly, as expected for the self-diffusion coefficient. At the very shortest times, however, the data for all volume fractions cannot be distinguished, within experimental uncertainty. As the time increases, the data begin to deviate from the limiting case of low volume fraction, with the data for the higher values of ϕ deviating at successively shorter time-scales. The data for the sample with the highest volume fraction, $\phi = 0.256$, appear to deviate at times considerably shorter than τ_v^0. For all ϕ, the approach to the asymptotic value of D_s is very slow.

To elucidate the behaviour further, we again numerically calculate the second derivative to obtain the velocity autocorrelation function for each value of ϕ, and plot these results logarithmically in Fig. 16.18. In each case, the velocity autocorrelation functions exhibit a power-law behaviour with the same exponent, $R(\tau) \approx \tau^{-3/2}$. This suggests that the functional form of each set of data is the same. To ascertain this, we use the functional form predicted for zero volume fraction, eqn (16.97), and use a non-linear least-squares fitting routine to compare this prediction with the data, allowing both the asymptotic value, D_s, and the time-scale, to vary during the fit. Very good agreement is obtained for
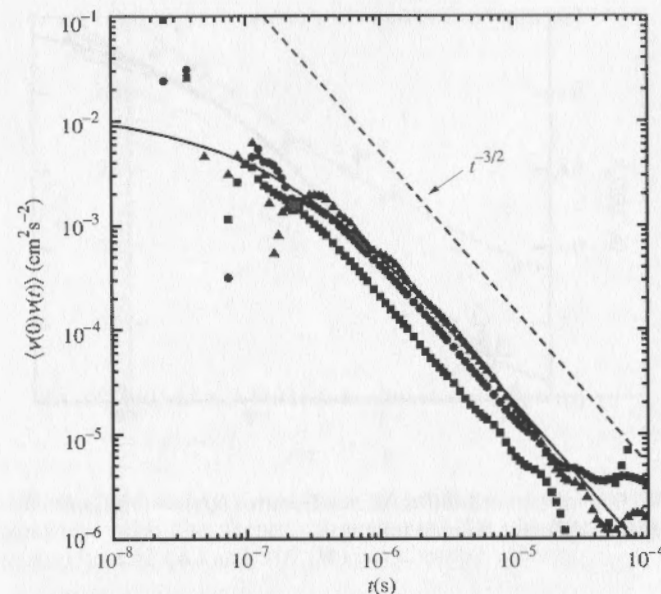
FIG. 16.18. Logarithmic plots of the velocity autocorrelation functions for 1.53 μm particles for volume fractions of (▲) 0.021, (●) 0.104, (■) 0.256. The $t^{-3/2}$ 'long-time tail' is apparent for each data set. The solid line is the calculation by Hinch[28] for the dilute-suspension limit.

each data set. Thus all the data can be scaled on to a single master curve, as shown in Fig. 16.19.

The parameters used to scale the data on to the master curve are obtained from the fit to the zero-volume-fraction form. The first parameter scales the data in the vertical direction, and provides a measure of the asymptotic value of the self-diffusion coefficient. The ϕ-dependence of this scaling parameter, normalized by $D_0 = k_B T/6\pi\eta_0 a$, is shown in Fig. 16.20. For comparison, we also plot the theoretically expected behaviour of the short-time self-diffusion coefficient as a function of ϕ. This theoretical prediction is in good agreement with tracer diffusion measurements of the short-time self-diffusion coefficient. As can be seen in Fig. 16.20, the value of D_s obtained from the scaling is in excellent accord with the expected behaviour.

The second parameter scales the horizontal axis, and provides a new time-scale. The ϕ-dependence of this new time-scale, normalized by τ_v^0, is shown in Fig. 16.21. The time-scale also decreases with increasing ϕ, but does so more rapidly than D_s. In Fig. 16.21 we also plot $\eta_0/\eta(\phi)$ as the solid line, where $\eta(\phi)$ is the theoretical prediction for the ϕ-dependence of the inverse of the high-frequency viscosity of the suspension, normalized by η_0, the zero-ϕ value. Remarkable agreement is found between this theoretical prediction and the
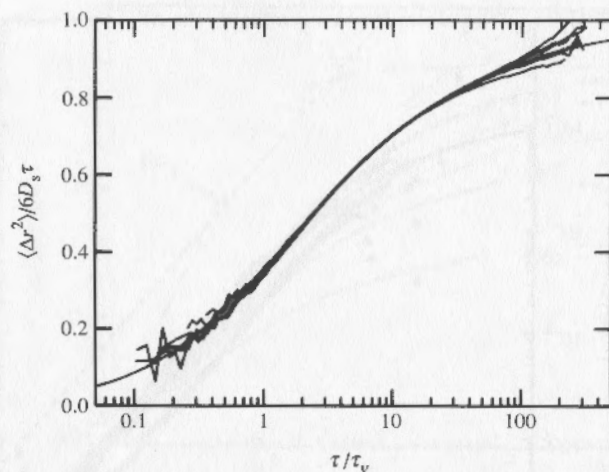
FIG. 16.19. Scaling of the self-diffusion coefficients, $D_s(t) = \langle r^2(t)\rangle/6t$, for data from 1.53 μm spheres at different volume fractions.
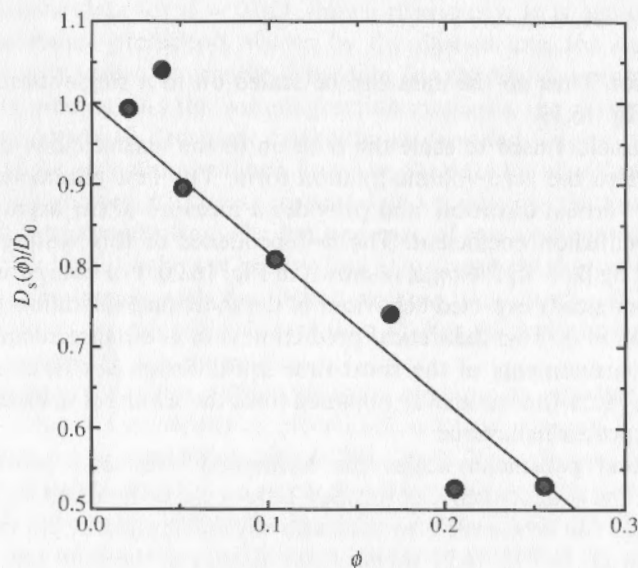

FIG. 16.20. Scaling parameter for the self-diffusion coefficient, normalized by D_0, as a function of volume fraction, compared with Batchelor's theoretical prediction, $D_s(\phi)/D_0 = 1 - 1.83\phi$ (solid line).[25]
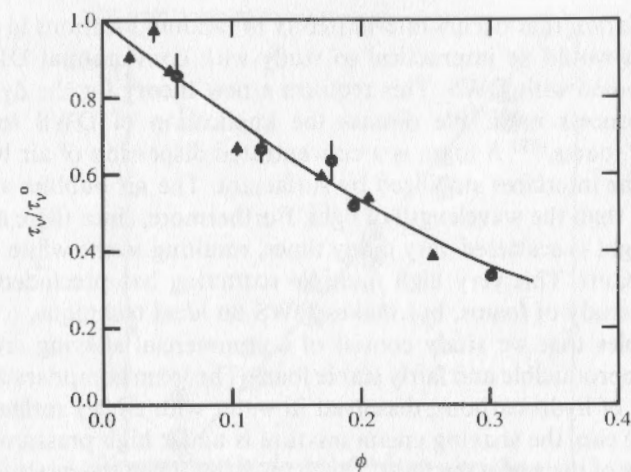
FIG. 16.21. Normalized scaling parameter τ_v/τ_v^0 for the time as a function of volume fraction, compared with the theoretical prediction for the normalized suspension viscosity $\eta_0/\eta(\phi)$ for 1.53 (▲) and 3.09 (●) μm diameter spheres.

measured time-scale. This suggests that the viscosity that determines the time-scale for the vorticity to diffuse away from a particle is the viscosity of the suspension itself. This behaviour is reasonable at later time-scales, after the vorticity has diffused over a large-enough length scale, so that the individual spheres cannot affect the viscosity. What is more surprising is the fact that the scaling behaviour holds to times as short as τ_v^0, where the vorticity has diffused a distance of the order of the sphere radius. Even at these time-scales, it seems that the effective viscosity is that of the suspension, rather than that of the pure fluid.

These measurements clearly demonstrate the power of DWS to study the behaviour of concentrated suspensions. Hydrodynamic interactions fundamentally affect all the dynamical properties of dispersions. They are also one of the most difficult and intractable problems in classical statistical mechanics. The ability of DWS to probe motion on such short length scales makes it possible to obtain a great deal of new information about hydrodynamic interactions. The results presented here demonstrate that it is now possible to observe experimentally the retarded nature of hydrodynamic interactions. In the future, DWS should allow a wide variety of new types of measurements to be performed, to probe motion on short length scales in many different systems. This will provide new challenges, both to experimentalists and to theorists.

16.3.4 *Foams*

In this section we discuss another application of DWS that takes advantage of the diffusive nature of the light paths, although in a completely different fashion.

We study motion that occurs intermittently in random locations in the sample. This motion would be impractical to study with conventional DLS, but can easily be studied with DWS. This requires a new theory for the dynamic light scattering process itself. We discuss the application of DWS to study the dynamics of foams.[29] A foam is a concentrated dispersion of air bubbles in a fluid, with the interfaces stabilized by surfactant. The air bubbles are typically much larger than the wavelength of light. Furthermore, since there are so many interfaces, light is scattered very many times, resulting in the white appearance typical of foams. This very high multiple scattering has precluded the use of DLS in the study of foams, but makes DWS an ideal technique.

The samples that we study consist of a commercial shaving cream, which provides a reproducible and fairly stable foam. The foam comprises a gas, which is a mixture of hydrocarbons, dissolved in water with added surfactant. While stored in the can, the shaving cream mixture is under high pressure, increasing the solubility of the gas in the fluid. The foam forms when the mixture is sprayed out of the can. The reduction in the ambient pressure reduces the solubility of the gas in the water, and small bubbles form. Initially they have a mean diameter of $\approx 20\ \mu m$, and a volume fraction $\phi \approx 0.92$. The bubbles all appear quite spherical under an optical microscope. Thus, in order to fill such a high volume fraction of space, the bubble size is necessarily not monodisperse. Instead there is clear distribution of sizes when the foam is first formed. As a result, the foam ages, or coarsens. The reduced radius of curvature of the smaller bubbles results in a higher pressure of gas inside them, compared with the larger bubbles, which have a larger radius of curvature and a correspondingly lower pressure. Thus gas can diffuse out of the smaller bubbles, causing them to shrink, and into the larger bubbles, causing them to grow. This coarsening process can be followed quite easily by multiple light scattering techniques.

The process of coarsening of the foam is relatively slow, and it can most readily be following by a static measurement, through monitoring the total amount of light transmitted through the foam. When the absorption of the sample is negligible, the total amount of light transmitted through a multiply-scattering sample is given by

$$T = \frac{5l^*/3L}{1 + 4l^*/3L}. \tag{16.99}$$

In the limit of a thick sample, $L/l^* \gg 1$, eqn (16.99) reduces to $T \approx 5l^*/3L$. Thus, knowing the sample thickness, the transmission provides a simple measure of the transport mean free path. This is a single length scale that parametrizes the transport of light through the medium. If the randomization of light in a foam is characterized by a single length scale, the only relevant length is the average bubble size. Thus the total transmitted light should provide a measure of the average bubble size in a foam through the measurement of the transport mean free path. To test this, we measure l^* in a sample of the foam
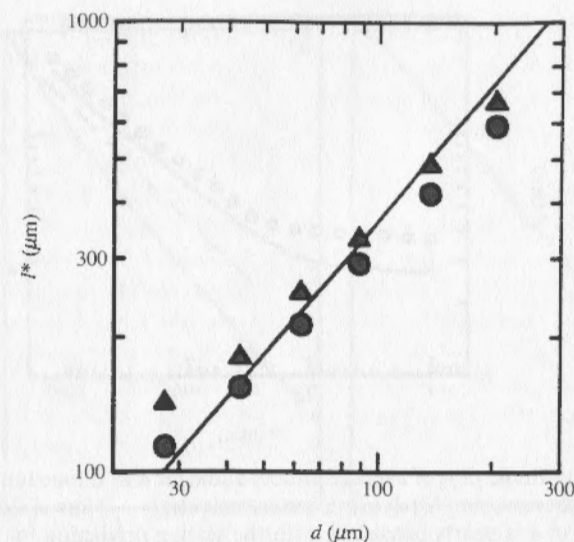
FIG. 16.22. Correlation between the measured value of l^* and the average bubble size as measured on the surface of a foam with a microscope: (●) static transmission measurements; (▲) dynamic DWS measurements.

by measuring the total transmitted light. Rather than attempt to collect all the transmitted light, we collect a small portion of the light transmitted in the forward direction, and compare this with the light transmitted through a sample of the same thickness, with a known l^*, measured with an identical optical arrangement. Then, by normalizing the two measured intensities, we are able to determine l^* directly. In Fig. 16.22, we compare the measured value of l^* with the average bubble size d as measured at the surface of the foam using a microscope. Nearly linear behaviour is observed, as shown by the solid line, confirming that l^* does provide a measure of the average bubble size. For this foam, the ratio gives $l^* = (3.5 \pm 0.5)d$, allowing l^* to be used to determine the average bubble size directly.

The ability to measure the average bubble size by measuring the transmitted light provides a simple method of following the coarsening of the foam. The time-dependence of the average bubble size is shown in a logarithmic plot in Fig. 16.23. After about 20 min, the growth of the average bubble size follows a power law in time, $d \propto t^z$, with $z \approx 0.45$. A power-law behaviour for the growth in the average bubble size for foams of this type is expected on the basis of a scaling picture which describes the effects of coarsening on the full distribution of bubble sizes. The distribution of bubbles is assumed to be statistically self-similar, so that the overall shape of the distribution, normalized by the average bubble size, remains the same as the foam coarsens. Then, if the bubbles are densely packed, the growth of the average bubble size is predicted to be a
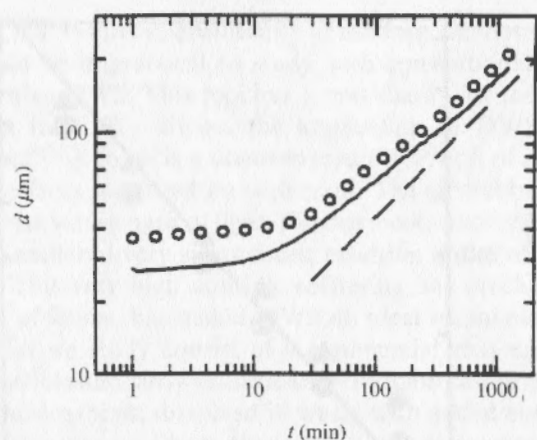
FIG. 16.23. Logarithmic plot of average bubble diameter d as a function of age of foam: (——) static measurements; ($\bigcirc$) dynamic measurements; (---) line of slope 0.5, showing that the growth of d is nearly consistent with the scaling prediction for densely packed bubbles.

power law in time, with a dynamic exponent of $z = 0.5$. There is a close analogy between this type of foam coarsening and the late stages of phase separation or of Ostwald ripening.

In addition to the static light transmission, there are also strong temporal fluctuations in the intensity of each speckle spot. Thus we can also perform DWS measurements, and measure the temporal autocorrelation function of both the transmitted and the backscattered light. Typical normalized field autocorrelation functions are shown in Fig. 16.24. Both sets of data were collected for 10 min after the foam had aged for about 100 min. In Fig. 16.24(a) we show a semilogarithmic plot of data obtained for light transmitted through a 0.3 cm thick cell, while in Fig. 16.24(b) we show the data collected in backscattering from a 1 cm thick cell, plotted as a function of the square root of time. The shapes of the autocorrelation functions in both cases are identical to those obtained from Brownian particles, as demonstrated by the fits to the data shown by the solid lines. The transmission data are fitted to eqn (16.41), while the backscattering data are fitted to eqn (16.46). The backscattering data yield a characteristic decay time, τ_0. This value can be used with the results of the fit to the transmission data to obtain a value for l^*. The value so obtained is found to be in excellent accord with that determined by the static transmission measurements. This is illustrated in Fig. 16.22 where the values of l^* obtained with the DWS measurements, represented by triangles, are compared with the values determined by the static transmission measurements, shown by circles. The two sets of data are in good agreement, demonstrating the consistency of our interpretation.
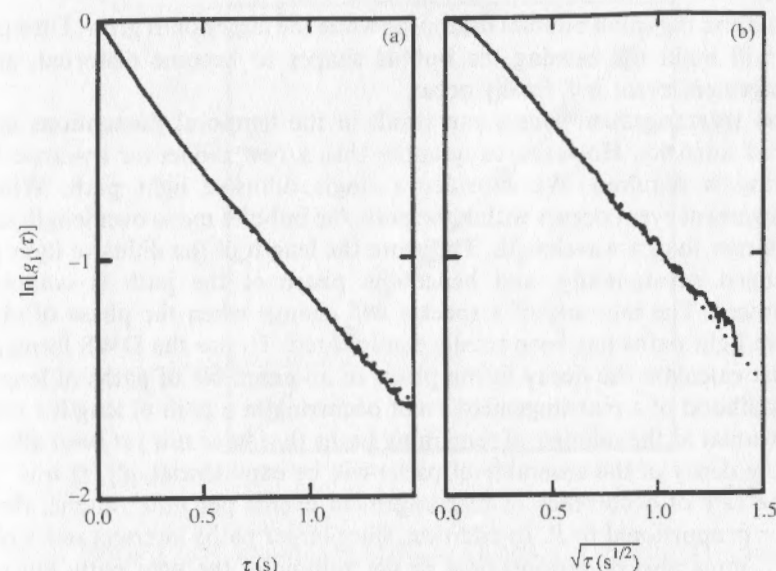
FIG. 16.24. Autocorrelation functions for foam for: (a) transmission through a 3 mm thick cell; (b) backscattering from a 1 cm thick cell. Both sets of data were collected for 10 min after the foam had aged for 100 min.

What is more surprising is the fact that the correlation functions have the same functional form as those obtained for Brownian particles. The foam bubbles do not undergo Brownian motion on a time-scale consistent with the measured correlation functions. In addition, other types of motion, such as the coarsening process itself, or fluctuations of the bubble interfaces due to capillary waves, would lead to very different shapes for the correlation functions, since these motions are not diffusive. Furthermore, the time-scales of these types of motions would be very different from that obtained from the data. Insight into the origin of the temporal fluctuations comes from observation of the surface of the foam with a microscope. Over longer periods of time, the coarsening of the foam is observed, with the average bubble size increasing, and with the smaller bubbles shrinking while the larger bubbles grow. On shorter time-scales, the bubbles are stationary, as the coarsening is too slow to observe directly. However, some motion of the bubbles is observed: there are discrete, random rearrangement events, in which several bubbles suddenly shift their positions. The rearrangement events extend over about 10 bubbles and last for about 0.5 s. Presumably these rearrangement events occur because of stresses built up as a result of the coarsening process. The volume fraction of bubbles, $\phi = 0.92$, is so large that the distribution of bubble sizes is essential to achieve such high packing volume fractions while maintaining spherical bubbles. If the local packing geometry is optimal at one time, it will not remain so as the foam

coarsens and the small bubbles disappear while the larger ones grow. Ultimately stress will build up, causing the bubble shapes to become distorted, and a rearrangement event will finally occur.

These rearrangement events can result in the temporal fluctuations in the scattered intensity. However, to quantify this, a new model for dynamic light scattering is required. We consider a single diffusive light path. When a rearrangement event occurs within the path, the bubbles move over length scales much larger than a wavelength. Therefore the length of the diffusive light path is changed substantially, and hence the phase of the path is completely randomized. The intensity of a speckle will change when the phase of all the diffusive light paths has been totally randomized. To use the DWS formalism, we must calculate the decay in the phase of an ensemble of paths of length s. The likelihood of a rearrangement event occurring in a path of length s will be proportional to the number of remaining paths that have not yet been affected. Thus the decay of the ensemble of paths will be exponential, $g_{(1)}^s(\tau) = e^{-\gamma_s \tau}$. If R is the rate of occurrence of rearrangement events per unit volume, then γ_s must be proportional to R. In addition, since larger paths intersect more of the foam, γ_s must also be proportional to the volume of the light path. Since the smallest meaningful length for diffusing light is l^*, the volume of the path is approximately $V_s \approx s l^{*2}$. Finally, since larger regarrangement events will affect more paths, we must include a factor which accounts for the efficiency for the events. We assume that each event involves bubble motion over a spatial extent r. Since the bubble rearrangement must occur over a volume of l^{*3} in order to totally randomize the phase of a path, we include a factor of $(r/l^*)^3$ to account for the efficiency of each event in dephasing the path. Thus we have $\gamma_s \approx R(s l^{*2})(r/l^*)^3$. The exponent of the decay of paths of length s is then linear in both s and τ. This is exactly the requirement for the DWS autocorrelation functions to have the shape predicted for Brownian particles. In addition, all the formalism developed for DWS for Brownian particles can be directly applied to foams. Thus, by comparison with eqn (16.46), we can identify $\tau_0^{-1} \approx R r^3$. Physically, τ_0 is the time between rearrangement events at any given point in the foam.

To test this picture for the origin of the fluctuations and for the DWS measurements, we again compare the light scattering results with optical measurements of the film surface made with a microscope. The rate of rearrangement events on the surface is determined with a microscope, assuming that we are able to observe events in the region of three bubble diameters into the foam. We then determine τ_0 from backscattering measurements and l^* from transmission measurements. If our model is correct, we expect $1/\tau_0 l^{*3} \propto R$. This is observed, as shown in Fig. 16.25 where we plot values of $1/\tau_0 l^{*3}$ measured by light scattering as a function of R measured at the surface of the foam. Excellent consistency is observed, as indicated by the straight line through the data, confirming our model for DWS from foams. Thus DWS can be used to probe the rate of bubble rearrangement events in the foam.
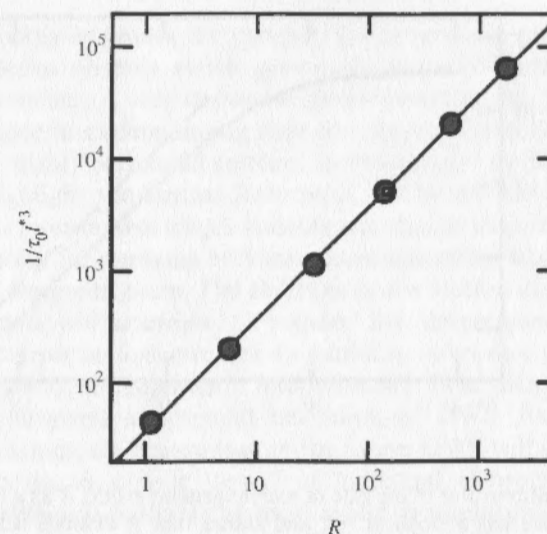
FIG. 16.25. Plot of $1/\tau_0 l^{*3}$ measured by DWS, as a function of the rate of rearrangement R measured at the surface of the foam with a microscope. The solid line is a best fit to the data.

The rate of rearrangement events in the foam is not constant in time, but instead decreases as the age of the foam increases. In Fig. 16.26 we show a logarithmic plot of R as a function of the foam age. A power-law behaviour is again observed at longer times, $R \propto t^{-y}$, with $y \approx 2.0 \pm 0.2$. The value of the exponent y is somewhat surprising. We expect that the rate of rearrangement events should decrease as the number of bubbles decreases. The number of bubbles scales inversely as the cube of the average bubble size. Since $d \propto t^{0.45}$, this would contribute a $t^{-1.35}$ time-dependence. We also might expect that a bubble rearrangement event would occur after the bubble size has increased by some fraction of its original size, consistent with a scaling picture of the foam behaviour. This implies that $\delta t/\tau_0 = \delta d/d$, so that $\tau_0^{-1} = (1/d)\frac{\mathrm{d}}{\mathrm{d}t}d$. Since $R \propto 1/\tau_0$, this gives $R \propto t$, regardless of the exponent for the time-dependence of d. Thus the exponent y should have a value of 2.35, somewhat greater than that observed. The only additional assumption that we make in obtaining this value is that the foam coarsening and dynamics can be described with a scaling picture, as suggested by the coarsening behaviour observed with the static transmission measurements.

With this new model for dynamic light scattering, DWS can be fruitfully applied to the study of foam dynamics. Other forms of foams will in all likelihood exhibit significantly different behaviour. For example, the coarsening process in other foams may be quite different: in this foam, we never observe the coalescence of bubbles during the coarsening. By contrast, many foams age
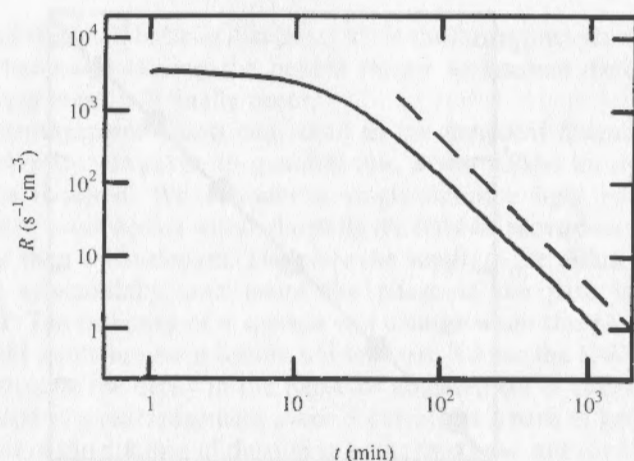
FIG. 16.26. Logarithmic plot of the rate of rearrangement events R as a function of foam age. The dashed line has a slope of -2 and shows that R exhibits scaling behaviour.

as the bubble walls break, leading to coalescence and coarsening. A good illustration of this type of coarsening is the foam on the top of a glass of beer. This process should also be directly observable using DWS. Furthermore, the rate of bubble rearrangement events must directly reflect the relaxation of stresses in the foam as the coarsening process proceeds. The stress will be relaxed as the bubbles move with respect to their neighbours. A similar type of motion will also occur when the bubbles move to relax a stress that is externally applied. Thus DWS may provide an ideal probe of bubble dynamics of the scale that is most important for the rheology of the foam. This holds great promise for applying DWS to a wide range of important problems in the study of foams.

16.1 Conclusions

In this chapter we have summarized recent developments in diffusing-wave spectroscopy, a new kind of dynamic light scattering which is suitable for studying opaque systems that exhibit a very high degree of multiple scattering. In reality, DWS is simply the extension of traditional dynamic light scattering to the multiple-scattering regime. However, the application of DWS requires a re-evaluation of how dynamic light scattering is used. The experimental set-up for DWS is substantially simpler than for traditional DLS. For example, no elaborate mechanism is required for precisely measuring and varying the scattering angle. Instead, the dynamical length and time scales are varied by working in either backscattering or transmission geometries and by varying the sample thickness. DWS opens up for study a whole new class of systems, and

in particular greatly improves the prospect for progress in understanding the dynamics of dense systems which previously were not amenable to light scattering experiments. A very important development in this respect has been the progress made in understanding how to interpret DWS data for strongly interacting and highly correlated systems. In this chapter we have used several examples to highlight the special features of DWS, specifically its utility in probing particle motion over length scales much smaller than the wavelength of light and its utility for studying systems whose dynamics, like those of foam, are spatially or temporally rare. The ability to probe motion at very short times has required and will continue to require the development of very fast correlators and associated electronics. In addition, novel new techniques, such as the application of the Michelson interferometer, offer alternative means of extending the temporal and spatial resolution of DWS. Besides the many scientific applications, we believe that in the future DWS will be very useful in process monitoring in a wide variety of industrial environments. In these applications, DWS will probably be most useful in monitoring *changes* in the system dynamics as a process proceeds. Thus one could monitor changes in particle size, aggregation, or gelation processes. These potential applications remain largely unexplored and may represent some of the most important future uses of DWS.

Acknowledgements

References

1. Ishimaru, A. (1978). *Wave propagation and scattering in random media*. Academic Press, New York.
2. Van Albada, M.P., van Tiggelen, B. A., Lagendijk, A., and Tip, A. (1991). *Phys. Rev. Lett.*, **66**, 3132.
3. Maret, G. and Wolf, P. E. (1987). *Z. Phys. B*, **65**, 409.
4. Pine, D. J., Weitz, D. A., Chaikin, P. M., and Herbolzheimer, E. (1988). *Phys. Rev. Lett.*, **60**, 1134.
5. Pine, D. J., Weitz, D. A., Zhu, J. X., and Herbolzheimer, E. (1990). *J. Phys. (France)*, **51**, 2101.
6. Stephen, M. (1988). *Phys. Rev. B*, **37**, 1.
7. MacKintosh, F. C. and John, S. (1989). *Phys. Rev. B*, **40**, 2838.

8. Pusey, P. N. and Tough, R. J. A. (1981). In *Dynamic light scattering: applications of photon correlation spectroscopy* (ed. R. Pecora). Plenum Press, New York.
9. Feng, S., Kane, C., Lee, P. A., and Stone, A. D. (1988). *Phys. Rev. Lett.*, **61**, 834.
10. Stephen, M. and Cwilich, G. (1987). *Phys. Rev. Lett.*, **59**, 285.
11. Carslaw, H. S. and Jaeger, J. C. (1990). *Conduction of heat in solids*, 2nd ed. Clarendon Press, Oxford.
12. MacKintosh, F. C., Zhu, J. X., Pine, D. J., and Weitz, D. A. (1989). *Phys. Rev. B*, **40**, 9342.
13. Fraden, S. and Maret, G. (1990). *Phys. Rev. Lett.*, **65**, 512.
14. Pine, D. J., Weitz, D. A., Maret, G., Wolf, P. E., Herbolzheimer, E., and Chaikin, P. M. (1990). In *Scattering and localization of classical waves in random media* (ed. P. Sheng). World Scientific, Singapore.
15. Watson, G. H., Fleury, P. A., and McCall, S. L. (1987). *Phys. Rev. Lett.*, **58**, 945.
16. Drake, J. M. and Genack, A. Z. (1989). *Phys. Rev. Lett.*, **63**, 259.
17. Yoo, K. M. and Alfano, R. R. (1990). *Optics Lett.*, **15**, 320.
18. Yodh, A. G., Kaplan, P. D., and Pine, D. J. (1990). *Phys. Rev. B*, **83**, 4744.
19. Middleton, A. A. and Fisher, D. S. (1991). *Phys. Rev. B*, **43**, 5934.
20. Ackerson, B. J., Dougherty, R. L., Reguigui, N. M., and Nobbmann, U. (1992). *J. Thermophysics and Heat Transfer*, (in press).
21. Kaplan, P. D., Yodh, A. G., and Pine, D. J. (1992). *Phys. Rev. Lett.*, **68**, 393.
22. Qiu, X., Wu, X. L., Xue, J. Z., Pine, D. J., Weitz, D. A., and Chaikin, P. M. (1990). *Phys. Rev. Lett.*, **65**, 516.
23. Xue, J. Z., Wu, X. L., Pine, D. J., and Chaikin, P. M. (1992). *Phys. Rev. A*, **45**, 989.
24. (a) Ashcroft, N. W. and Langreth, D. C. (1967). *Phys. Rev.*, **159**, 500.
    (b) Ziman, J. M. (1961). *Phil. Mag.*, **6**, 1013.
25. Batchelor, G. K. (1976). *J. Fluid Mech.*, **74**, 1.
26. Yodh, A. G., Georgiades, N., and Pine, D. J. (1991). *Optics Commun.*, **83**, 56.
27. Horne, D. S. (1989). *J. Phys. D: Appl. Phys.*, **22**, 1257.
28. Hinch, E. J. (1975). *J. Fluid Mech.*, **72**, 499.
29. Durian, D. J., Weitz, D. A., and Pine, D. J. (1991). *Science*, **252**, 686.